ABSOLUTE RADIOMETRIC CALIBRATION OF AN ON-ORBIT INFRARED SENSOR USING STARS

Thesis

Submitted to

The School of Engineering of the

UNIVERSITY OF DAYTON

In Partial Fulfillment of the Requirements for

The Degree

Master of Science in Electro-Optics

by

Mark Donofrio

UNIVERSITY OF DAYTON

Dayton, Ohio

December 1996

ABSOLUTE RADIOMETRIC CALIBRATION OF AN ON-ORBIT INFRARED SENSOR USING STARS

APPROVED BY

ABSTRACT

ABSOLUTE RADIOMETRIC CALIBRATION OF AN ON-ORBIT INFRARED SENSOR USING STARS

Name: Donofrio, Mark
University of Dayton, 1996

Advisor: Dr. G. R. Little

This thesis addresses the absolute radiometric calibration of an infrared sensor that is already on orbit. Stars located in the Southern sky are approximated as blackbody sources in the near infrared portion of the electromagnetic spectrum (i.e. 2.0-3.5μm) and used to measure the absolute response of each pixel on a 16 x 16 Mercury-Cadmium-Telluride (HgCdTe) focal plane array. Since the sensor is equipped with a six-position filter wheel (five spectral bands and one opaque position), the pixels are also spectrally dependent. Stars of different spectral classes (i.e. temperature) and magnitudes (i.e. radiant flux) are used to create a broad selection of data. In turn the data is used to validate the conversion constants that relate the sensor count value to a radiant flux ($W/cm^2/\mu m$) for each of the four primary bands. Predictions are based on the Engelke normalized blackbody function and converted to sensor counting units for direct comparison with actual measurements [1, 2]. A sum-of-nine pixel centroid is calculated for each frame of measured data and an attempt

is made to assess the accuracy and consistency of the absolute response correction factors for all pixels in the four spectral bands. Conclusions on the current uniformity of the focal plane array, accuracy of the voltage to flux conversion constants, and recommendations for future radiometric calibrations of similar on-orbit sensors are included as well.

ACKNOWLEDGMENTS

I would like to thank several key individuals who made this thesis work possible. In particular, Dr. Gordon Little, my advisor, for providing the necessary oversight of my work and taking the extra time to learn about the sensor calibrated. In addition my sincerest thanks to Mr. James Lisowski for his endless enthusiasm and dedication to this project.

I would also like to express my appreciation to several other people who contributed to this effort. Mr. Brett Borowski provided the computer programming expertise for the data processing software. Mr. Robert Cody offered guidance with the sensor performance and anomalies. Mr. James Engel advised on the technical aspects of the sensor. Mr. Wilbur Dong provided personal contacts and unpublished reports for star radiant flux density predictions. Mr. William Parker tasked the sensor for each collection and resolved any scheduling conflicts. Finally, the time required to complete this thesis would not have been possible without the support and patience of both my wife, Andrea, and my daughter, Megan. This report is first and foremost dedicated to them.

PREFACE

Space based sensors are normally calibrated in a laboratory environment prior to deployment to orbit. In the case of this sensor, aggressive launch schedules and other priority items severely restricted the amount of absolute calibration performed on the ground. Coupled with the detection of new and unique targets over the past few years, the need arose for an absolutely calibrated focal plane. This thesis is an attempt to satisfy that need and identify improvements for future calibrations.

TABLE OF CONTENTS

LIST OF FIGURES

LIST OF TABLES

LIST OF SYMBOLS/ABBREVIATIONS

CCD	Charge Coupled Device
epro	End Product (Data File)
HgCdTe	Mercury-Cadmium-Telluride
IR	Infrared
LD	Level of Detection
SWIR	Short Wave Infrared
λ	Wavelength (in μm)
Ω	Solid angle subtended by star
E	Radiant flux (of star)
E_{ngelke}	Engelke function-derived radiant flux
E_0	Radiant flux of star at λ=0.55μm
I	Irradiance (of star)
K	Kelvin
L_λ^b	Blackbody spectral radiance
R	Absolute responsivity of sensor
S_λ	Visible response function
$S(\lambda)$	Sensor filter response function
T_B	Brightness temperature
T_e	Effective (published) temperature

CHAPTER I

INTRODUCTION

The sensor addressed to in this thesis requires on-orbit radiometric calibration to correctly identify the one-of-a-kind targets it detects. A more detailed description of the sensor is included in Appendix A. Most often these targets are sensed against a "warm" earth background and extensive post-processing is required to extract low intensity targets from the existing background clutter level. If the absolute response for each pixel of the sensor's focal plane array is successfully determined for each spectral band, then a larger portion of the clutter level could be subtracted from the remaining signal during post-processing to obtain a more accurate photon count for a given target.

Because the sensor has already been deployed to orbit, normal laboratory techniques for calibration cannot be followed. For example, calibrated laboratory blackbody sources that are set to radiate at known temperatures could not be used to create a response on the sensor's focal plane array. On-orbit calibrations require the use of either a high powered laser or some other existing "hot" source. Stars were chosen as the radiation source because they are readily accessible and can be used repeatedly for re-calibration of the sensor with minimal effort. Stars are desirable because they are point sources, radiate similarly to a blackbody, and can be measured against a very cold, low clutter background. Appendix B addresses reasons for treating stars as

blackbody sources for this particular sensor. The blackbody approximation for stars is especially true for those that do not show emission lines associated with Carbon and other elements. Additionally, the point source-like nature of the stars will be used to address the uniformity of the focal plane and can also be used for concurrent work with pixel gap analysis and modeling.

To determine the set of stars to use for calibration, several preliminary steps were completed. These include: 1) determining whether the sensor could view the star based upon the sensor's orbit and its slewing ability, 2) testing whether or not the star's intensity was large enough to be detected by the focal plane and successfully extracted from the noise level in each spectral band, 3) researching the star's associated spectral database and determining whether it approximated a blackbody in the short-wave infrared (SWIR) region, and 4) using a modified blackbody curve to predict the response for the chosen stars in each sensor band.

The first task was accomplished with the help of a computer algorithm developed by the sensor's collection organization. This program models the sensor's orbit and slewing capabilities for a given date and time and calculates a region of right ascension and declination values in the field of view of the sensor. For the time period this estimation was made, the sensor was able to view a right ascension between 220 and 290 degrees and a declination between -34 and -70 degrees [3]. Except for areas where the earth obscured the view of a star, this is the region where the candidate stars were chosen. This region limited the number of traditionally popular infrared calibration stars, such as Vega, that are located in the northern sky. However, several stars in the southern sky, referred to as "standards for IR calibration" in published

documents such as the Massachusetts Institute of Technology Lincoln Laboratory's "Proposed Astronomical Reference Catalog of Infrared Sources" [4], were used. The Engelke report [2] contained a similar list of standard stars and was also used to create a list of candidate calibration stars for this sensor. Table 1 shows the initial list of the stars chosen for calibration measurements. This list was later condensed to four primary stars based on the amount of radiometric information available in open literature for radiometric flux predictions and the window of opportunity for viewing the star throughout the year. These criteria significantly impact the potential for future calibrations and improvements in the accuracy of the results.

Table 1 - Initial stars for sensor calibration

Star	RA (1993)	Dec (1993)	Spectral Type	IR Standard[4,2]
λ Vel	136.939	-43.406	K4 Ib	Yes[2]
μ Vel	161.622	-49.386	G5 III	No
2 Cen	207.267	-34.419	M4 III	Yes[2]
α Cen	219.785	-60.811	G2/K1 V	Yes[4,2]
γ Cru	187.700	-57.077	M3 III	Yes[4,2]
ε Sco	252.435	-34.282	K2 III	Yes[4]
β Ara	261.190	-55.524	K3 IIb	Yes[4]
η Sgr	274.297	-36.764	M3 III	Yes[4,2]

The next step toward prediction of a star's spectral radiance in a specific sensor band involved a literature search of available data on each of the candidate stars for the calibration. However, an extensive search of literature from NASA and other astronomical databases yielded only marginal spectral data for popular stars such as Alpha Centauri, and little or no data for M-type stars such as 2 Centauri and Gamma Crucis. It turns out that only a limited amount of actual high resolution spectral structure for southern stars has been made above the atmosphere and below a wavelength of 5μm [6]. For example, NASA's Infrared Astronomical Satellite (IRAS) has measured the flux from

several thousand stars in all regions of the sky. Unfortunately, its primary spectral bands are at 12μm and 25μm and no data is published for this system below 5μm, especially to the level of detail required for absolute calibration ($\Delta\lambda$~0.05μm). More measurements may be available from ground based observatories, however the transmission codes (e.g. MODTRAN, LOWTRAN) used to remove the signal attenuation due to the earth's atmosphere are not exact. In addition, if the weather at the time of the observation is not accurately characterized the signal may differ considerably from the actual radiant flux density received at the telescope aperture. As a result, ground based data for a continuous spectral range were ruled out as an accurate source of information.

Discussions with M. Cohen [7] revealed work is being done to record high resolution spectral data from primary IR calibration stars (Alpha Centauri included). While the high altitude Alpha Centauri data acquired from this effort may benefit future calibrations of the this sensor, the data was not yet published and available for use at the time of this report.

Based on the modified blackbody function for each star, a summation was performed with the response function for each of the four sensor bands. Each intensity value was then converted to the sensor Level of Detection (LD) counting unit for each band. The relationship between radiant flux density and LDs is linear and the mathematical relationship is included in Chapter 2.

Based on past experience, the noise level of the sensor and other jitter or pointing errors normally restrict the star detection threshold to approximately 100 LDs [8]. The LD values obtained for each star were also used to determine the range of source intensities used. This could provide insight into the linearity of

the HgCdTe focal plane in detecting both dim (hundreds of LDs) and bright (thousands of LDs) sources.

Following these preliminary calculations, data acquisitions were made. In order to acquire good data, the sensor scanned slowly across the sky so each star was moved across the entire focal plane, with approximately 15 "hits" on each pixel for every pass made. The downlinked focal plane data was then transmitted to the ground and analyzed on a Silicon Graphics workstation. A software program then processed the individual data files into a single matrix containing the average sum-of-nine value for each pixel. The results are displayed in the form of 16 x 16 matrices showing LDs versus pixel location. The LD values for each pixel were then compared to the predicted star LDs for each sensor band. Since a linear response from each pixel is idealistic, a discussion of the potential factors affecting the sensor follows the analysis of results.

This type of calibration may be repeated for this and similar sensors. A key factor in the accuracy and consistency of this work was selecting a range of infrared stars that: 1.) fell within the sensor's viewing geometry, 2.) did not show significant variation over time, 3.) registered at least 100 LDs on a given pixel in each spectral band and 4.) remain in the sensor's field of view for a majority of the year to enable re-calibration on an as needed basis in the future.

Absolute radiometric calibration of this sensor is extremely valuable to the organizations who rely on the data from this sensor. Data collected is currently processed under the assumption that the focal plane has an identical response for each pixel. This report provides a means for characterizing the internal noise

of the sensor. It also compliments other studies performed on this sensor, such as relative pixel response corrections (focal plane nonuniformity corrections) and pixel gap analysis [9].

CHAPTER II

BACKGROUND

All matter in the universe at a finite temperature radiates energy. This energy is, in turn, transferred to other bodies that either absorb and/or reflect certain amounts of the radiation. For this reason the signal recorded on the detectors is composed of two separate elements that must be accurately separated in order to reach an acceptable level of calibration. These elements are commonly referred to as signal and noise. The signal contains only the source energy while the noise (or background) incorporates all of the additional radiation falling on the detectors from other sources. Herein lies the fundamental principle of data processing, namely, characterizing the background radiation and removing it from the total signal on the focal plane to obtain an accurate measurement of the source radiation only. The amount by which the signal strength exceeds the noise radiation is known as the signal to noise ratio. In this experiment, radiation is collected from a star against a cold background at a sensor located in an orbit above the earth's atmosphere. Although the primary source of radiation on the detectors is the energy emitted from the star, there are other secondary sources of background noise that must be accounted for, either quantitatively or qualitatively.

A blackbody is an object that reflects none of the radiation incident upon it. As a result, it contains (ideally) no absorption lines that may lead to an inaccurate prediction of the radiation received at the sensor aperture. Celestial radiation sources that closely approximate this type are used for calibration of

the sensor. Blackbody sources emit their maximum amount of radiation at a wavelength inversely proportional to the temperature of the source. This maximum value is predicted by Wein's Displacement Law and is given by:

$$\lambda_{max} \times T_e = 2.8978 \times 10^{-3} \quad (1)$$

where λ_{max} is the peak wavelength of the blackbody function and T_e is the effective temperature (commonly referred to as simply the "temperature") of the source.

Furthermore, the spectral radiance distribution for a blackbody is given by the Planck Radiation Law [10]:

$$L_\lambda^b = \frac{c_1}{\pi\lambda^5\left[\exp\left(\frac{c_2}{\lambda T_e}\right) - 1\right]} \quad (2)$$

where c_1=1.1910x10^{4}J-m^2/s and c_2=1.4388x10^{4}J^2-m/K.

This equation gives the radiant flux density at the source, and is useful only if both the star size and distance from the star to the sensor are known. Commonly these distances are only estimated to one or two significant figures. Rather than introduce this substantial amount of uncertainty into the calculation of radiant flux received at the sensor's aperture, an equation that did not specifically include these parameters was used.

This calibration treats the stars used as being idealized sources. An isotropic point source has the same intensity when viewed from all possible directions. This approximation also neglects any physical dimensions of the star. The brightness of celestial bodies is normally reported in magnitudes. The scale is defined so the irradiance received just above the earth's atmosphere

from a star is related to a reference star irradiance given by the following expression:

$$I(m_2) = I(m_1)10^{0.4(m_1 - m_2)} \qquad (3)$$

where $I(m_1)$ and $I(m_2)$ are the irradiance values corresponding to the respective magnitude values m_1 and m_2

Magnitudes are documented primarily for the visible wavelength of 0.55μm. However, further research led to published magnitudes for the stars used in this experiment in the short wave infrared (SWIR) spectrum. They are based on a reference star that has an in-band flux of the value given in Table 2 below [10].

Table 2 - Zero magnitude spectral flux density for standard astronomical bands

Band	λ_c (μm)	$\Delta\lambda_c$ (μm)	Flux (m_v=0) W/cm^2/μm
V	0.55	0.089	3.72×10^{-12}
H	1.65	0.30	1.28×10^{-13}
K	2.22	0.48	4.14×10^{-14}
L	3.60	0.70	6.38×10^{-15}
M	5.0	1.73	1.82×10^{-15}

Emission from a star is also characterized by spectral types. The majority of stars (~99%) are classified by the designators O, B, A, F, G, K, and M, while the remaining, extremely rare stars use other letters. The major distinctions between classes are the star temperature and the types of emission lines, if any, in its spectrum.

Two methods used to calculate the expected star radiance at the aperture of the sensor are described below in the order of increasing accuracy. Each method is published in open literature, though not all are dependent on the same variables. The first estimate of star radiance could be made using Planck's

blackbody function. A method outlined by W. D. Dong [11] assumes the star is an ideal blackbody and calculates the star's spectral radiance over a given bandwidth. He uses the known visible flux (at λ=0.55μm) for establishing the normalization to obtain absolute flux values. The visible in band flux is determined using the apparent visible magnitude and incorporates the effects of both absolute brightness and distance to the star. The radiant flux received at the sensor's aperture from the star is expressed, mathematically, as:

$$E = E_0 \left(\frac{\int_{\lambda_1}^{\lambda_2} L_\lambda^b(T_e)\,d\lambda}{\int_0^\infty S_\lambda L_\lambda^b(T_e)\,d\lambda} \right) 10^{-0.4 m_v} \qquad (4)$$

where E_0 is the energy corresponding to a star of magnitude zero (equal to 3.7338×10^{-13} watts/cm^2) [12,13], S_λ is the wavelength dependent visible response function [14], λ_1 and λ_2 are the lower and upper bounds of the bandwidth, respectively, and m_v is the published magnitude of the star in the visible band (λ=0.55μm). Although this is the most straightforward calculation for determining the radiance from the star, Dong notes this approach may not be adequate for radiometric calibration, due to the estimation accuracy of extrapolating the visible magnitude of the star into the infrared region.

In a technical report published by the Massachusetts Institute of Technology Lincoln Laboratory, C. W. Engelke [1, 2] explains a more accurate function for calculating the spectral radiance from a star. In the report he develops a continuous function and uses iterative, computer-based calculations to fit a blackbody curve to actual spectral measurements at specific wavelengths. More specifically, the function uses stars that have been directly calibrated against a blackbody source to obtain known values of spectral flux at specific

wavelengths. These directly calibrated stars (i.e. Vega, Pollux, and Capella) then serve as a basis for stars lacking actual spectral flux values. A list of primary stars (spectral type A-K) and secondary stars (spectral type M) that accurately model a blackbody, taken from the Engelke appendix report by Reicke [2], are used to determine the overall accuracy of this method. Engelke also includes a list of stars in the Southern Hemisphere (the only valid sources for calibration of this sensor), based on both the primary and secondary lists, that are expected to yield flux values within five percent below 20μm. He reports this approach is accurate for stars "with smooth infrared spectra showing no evidence of excess emission from circumstellar dust clouds." The equation is:

$$E_{ngelke} = \Omega \times \int_{\lambda_1}^{\lambda_2} L_\lambda^b(T_B)d\lambda \qquad (5)$$

where the added constant Ω is the solid angle subtended by the star in steradians. This parameter is used to normalize the curve against specific measured quantities of the radiant flux from the star and is not a physically measured angle. The variable T_B is referred to as the brightness temperature of the star and is defined as:

$$T_B = 0.738\lambda T_e\left(1+\frac{79450}{\lambda T_e}\right)^{0.182} \qquad (6)$$

The brightness temperature is introduced with the knowledge that radiation from stars can penetrate further through the stellar atmosphere at shorter wavelengths in the infrared. This enables the original Planck blackbody function to model the actual solar (and other stellar) spectrum more closely. This temperature function therefore indicates the spectral flux of a star decreases more rapidly with increasing wavelength than an ordinary blackbody curve of the same temperature. The value of T_e therefore adjusts the overall shape of the spectral curve. [1]

Table 3 shows the values of the Ω and T_e constants for each star as published in the Engelke report. The Ω value for Lambda Velorum is not included here since it was not included as a primary star in the report. This value was therefore calculated by the author of this calibration report. It was obtained using a simple average over specified wavelengths where published data was available yielded a value for Ω of 10.72×10^{-15} steradians for Lambda Velorum. A summary of this calculation is provided in Appendix C as a reference.

Table 3 - Published solid angle and effective temperature constants for Engelke Function calculation.

Star	Ω (10^{-15} sr)	T_e (K)
α Centauri A	1.324	5870
α Centauri B	0.688	5060
2 Centauri	3.750	3310
γ Crucis	13.74	3410
λ Velorum	(not given)	4279

The Engelke Function is reported to be valid for wavelengths between 2 and 100 microns and stars of spectral type G through K. The function may need to be modified for stars of spectral type M not specifically called out in his report. However, Engelke specifically evaluates the flux of two M-type stars used in this effort. They are 2 Centauri and Gamma Crucis. He reports this modified blackbody function estimates the in-band flux density of these stars to within three percent of error margin. The report includes functions for Alpha Centauri, 2 Centauri, and Gamma Crucis. These stars were in the sensor's field of view and therefore suitable for calibration. A similar curve was also developed for Lambda Velorum, using the same technique, although the iterative curve fitting

process was not followed since the computer algorithm used by Engelke was unavailable. A degradation in the accuracy of the predicted LDs from Lambda Velorum is therefore expected. It is included because it provides insight into the accuracy of estimating spectral continuum from other stars not mentioned in the Engelke report for future calibrations. Since no actual spectral data are available for these stars, this report uses the Engelke Function to calculate the expected absolute flux of each star on the focal plane of the sensor for each spectral band. Future flux measurements and expanded star databases may, however, yield more accurate predictions of these values as well as improved calibration accuracy.

The celestial background is also an important consideration in calibration. However, according to D. Kryskowski and G. H. Suits [10] the "infrared emission from solid material (dust, ice, metal, condensates, etc.) distributed throughout our galaxy becomes increasingly important at wavelengths longer than about 4 μm". Since this calibration is performed at wavelengths shorter than 4 μm, these effects are minimal and would not introduce a significant amount of error into the measured LD values. The result is nearly zero background from space with the data processing technique outlined in Chapter III. They also state the infrared flux from most main sequence stars (A through M dwarfs) is well represented by the blackbody distribution at the star's published temperature. Most non-standard emission spectra are a result of carbon and silicates present in a cloud or shell surrounding the star. These effects are mostly present at 1.9μm and 2.7 μm wavelengths and would affect primarily band 3.

The above mentioned calculations and discussion of background effects lead to the predicted radiant flux values for each star in each sensor band.

Table 4 contains these numbers and they are used to determine the expected sensor count (LD) value for each case.

Table 4 - Predicted flux values calculated by correlating Equation (5) with the published sensor responsivity curves

Star	Band	Flux (10^{-14} W/cm^2/μm)
2 Centauri	1	4.88
2 Centauri	2	3.54
2 Centauri	3	4.23
2 Centauri	4	1.39
Alpha Centauri	1	4.47
Alpha Centauri	2	3.10
Alpha Centauri	3	3.56
Alpha Centauri	4	1.13
Gamma Crucis	1	1.82
Gamma Crucis	2	1.32
Gamma Crucis	3	1.57
Gamma Crucis	4	5.14
Lambda Velorum	1	15.15
Lambda Velorum	2	10.84
Lambda Velorum	3	12.78
Lambda Velorum	4	4.15

As explained in Chapter 1, this particular sensor uses a digital counting unit called a LD. After background subtraction, a LD is directly proportional to the spectral radiant intensity value (normally in watts per steradian per micron) detected on a given pixel. All sensor values presented in this report use LDs to prevent the release of sensor parameters that are sensitive and/or proprietary information.

An LD corresponds to the actual digital count from a given detector on the focal plane array. It is related to the in-band radiant flux (in W/cm^2/μm for the purposes of this experiment) by the following equation [15]:

$$LD = R \times 204.75 \times \Delta t_{int} \times \int_0^{\infty} S(\lambda) E_{ngelke}(\lambda) d\lambda \quad (7)$$

where R is the absolute responsivity constant of the sensor (measured by the manufacturer prior to deployment), 204.75 is the LD to volt conversion factor reported by the focal plane manufacturer and Δt_{int} is the integration time of the sensor (equal to 9.21×10^{-3} seconds). The values $S(\lambda)$ and $E_{ngelke}(\lambda)$ inside of the integral sign refer to the spectral responsivity of the filter used and the predicted data values for the radiant flux of the star, respectively. Note $S(\lambda)$ is different from the constant S_λ introduced earlier in this report.

However, current data processing techniques for this sensor assume the $S(\lambda)$ factor is a flat and absolute distribution for each filter. This idealization does not, however, hold true for absolute measurements with the sensor. As a result, the absolute calibration of this sensor is performed more accurately by comparing LDs predicted to LDs collected. By comparing LDs directly the conversion factors between radiant flux and LD counts for each filter wheel are calibrated with a minimal amount of error. The predicted LD values expected from each star in each band are included in Table 5 below. The prediction values in LDs for each case are also shown across the entire focal plane array in Appendix G to illustrate which pixels fall within the field of view of this telescope and therefore are considered "active" for calibration.

Table 5 - Predicted sensor count values calculated from Table 4 flux values and Equation (7)

Star	Band	Sensor Count (LDs)
2 Centauri	1	188
2 Centauri	2	137
2 Centauri	3	163
2 Centauri	4	53.6
Alpha Centauri	1	173
Alpha Centauri	2	120
Alpha Centauri	3	137
Alpha Centauri	4	43.4
Gamma Crucis	1	702
Gamma Crucis	2	508
Gamma Crucis	3	605
Gamma Crucis	4	198
Lambda Velorum	1	584
Lambda Velorum	2	418
Lambda Velorum	3	493
Lambda Velorum	4	160

A schematic drawing of the sensor's analog-to-digital unit conversion is shown in Figure 1 below. Photons incident on the telescope aperture are focused onto the focal plane array using a series of lenses. The beam is also split (spectrally) and the SWIR energy is directed through a six position filter wheel to determine the spectral band collection. Once the data is collected on the focal plane, it is converted to an electric signal using a bias voltage and then stored in a capacitor. The capacitor discharges 10 volts at a rate of 320 times every second and stores the energy in a 12 bit processor as a subframe analog to digital conversion. The highest and lowest value is then deleted and the signal is further divided into a 17 bit processor that enables the recorded signal to fit into a 16 bit word for electronic transmission to the ground. Once the signal reaches the 17 bit processor it is measured and recorded in units of LDs. The

data is recorded on a pixel by pixel basis so as to preserve the location information of the signal [15].

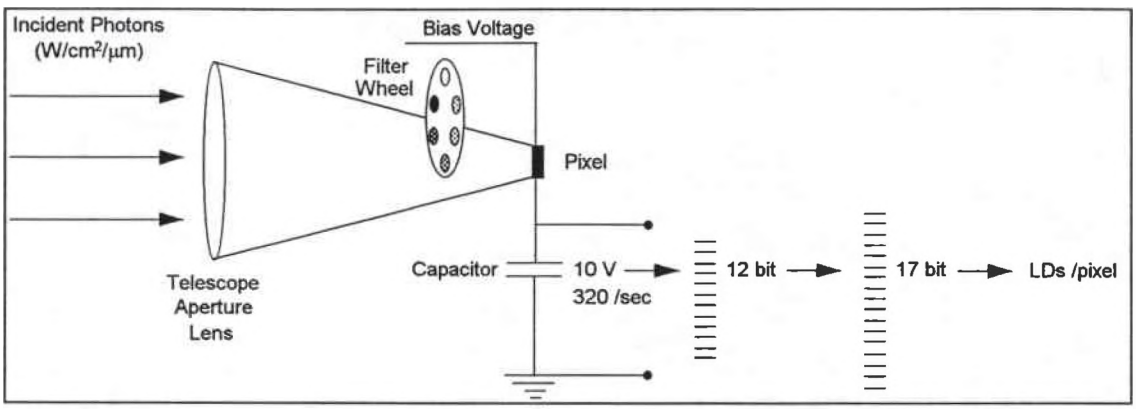

Figure 1 - Schematic drawing of sensor signal processing

The focal plane array consists of a 16 x 16 matrix of pixels. The telescope's field of view does, however, limit the amount of detectors that are able to receive incident energy. The result is a near circular shape of active pixels on the focal plane which are used to collect measurements. The pixels outside of the field of view are considered inactive and return no voltage signal to the capacitor. An illustration of the focal plane array is shown in Figure 2 below.

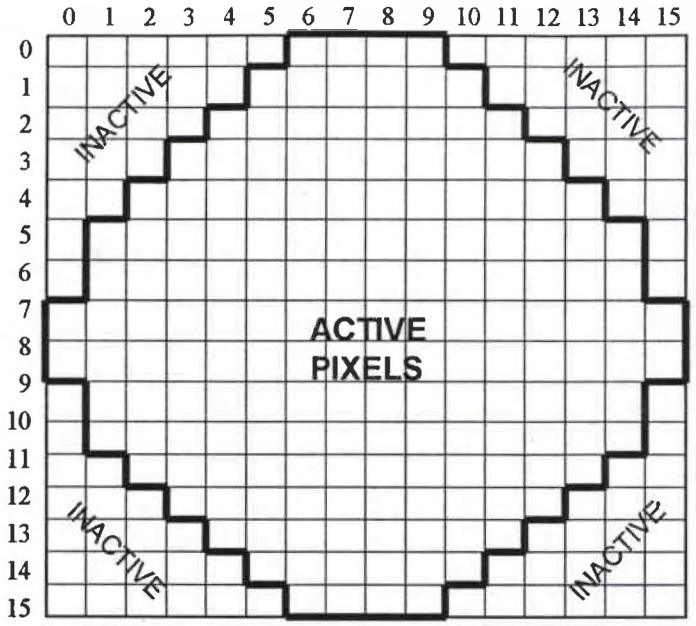

Figure 2 - Location of active and inactive pixels on the focal plane array

The fundamental constant for calibration of this sensor is the absolute responsivity. The expression for the absolute responsivity of an electro-optical sensor is written as:

R = (output voltage from detector) / (radiant power incident on detector).

Although this value was measured in the laboratory on the ground, this value may have changed over the several years since the sensor was deployed. It is therefore necessary to adopt an accurate and repeatable calibration experiment that gives insight into how this conversion factor may be changing over time, both spatially and spectrally. Additionally, the absolute responsivity constant can be used to estimate the Noise Equivalent Power (NEP) of the sensor. Wyatt defines this value as "the incident power required to produce an output voltage equal to the electrical noise voltage." and may be interpreted as "an input power that produces a change in the mean (rms) output signal equal to the standard deviation of the output noise" [16]. Note that the standard deviation

of the background is different from the initial background level subtracted at the beginning of sensor data processing where electronic and other bias noise effects are subtracted from the measured signal value. The accuracy of these measurements would quantify the effectiveness of system background noise characterization and removal from star data.

CHAPTER III

EXPERIMENT

The star data used for this calibration effort were collected between August 1995 and January 1996.

The first set of collections made of stars new to the sensor database were used to estimate the response from each source. If the signal received by the sensor from the star was large enough to detect and track, then this star was identified as a candidate for calibration. On the other hand, if the star was unable to be detected, using a simplified background subtraction program, then it was not used.

The actual collection files used for calibration of the sensor are listed in Appendix D of this report. These collections were made by moving the sensor telescope in a scanning pattern whereby the star was translated across a certain number of rows or columns of the focal plane array. A notional scanning pattern for the entire focal plane array is shown in Figure 3. Ideally, the data collection file should include a scan of every active pixel on the focal plane. However, due to available time windows for collection of star calibration data, (primarily a scheduling and priority issue) at least two collection files were required to collect measurements for every pixel.

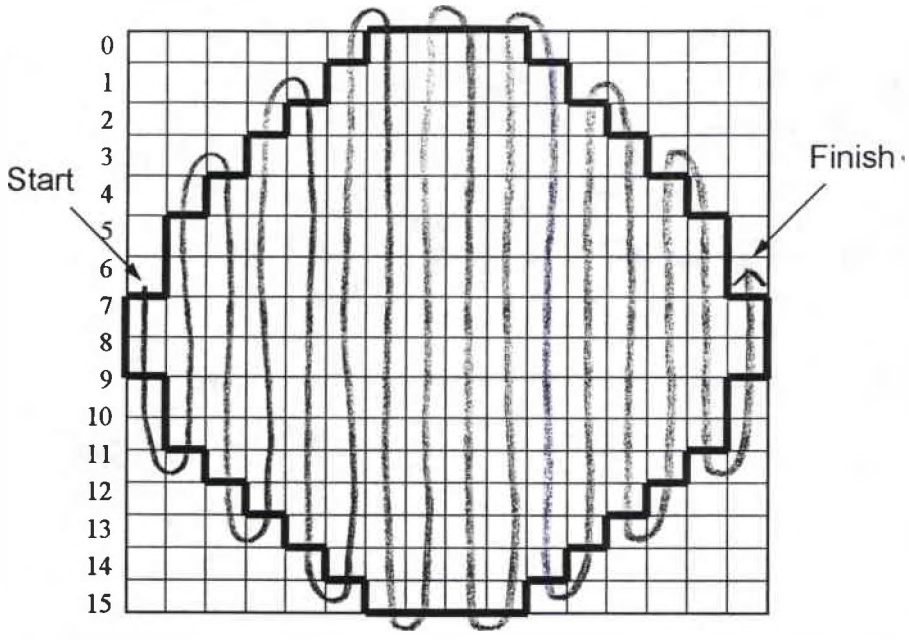

Figure 3 - Notional scan pattern for star measurements

A more specific illustration of how the star was translated across individual pixels is included in Figure 4, where the enlarged region represents four pixels and each point represents a measurement.

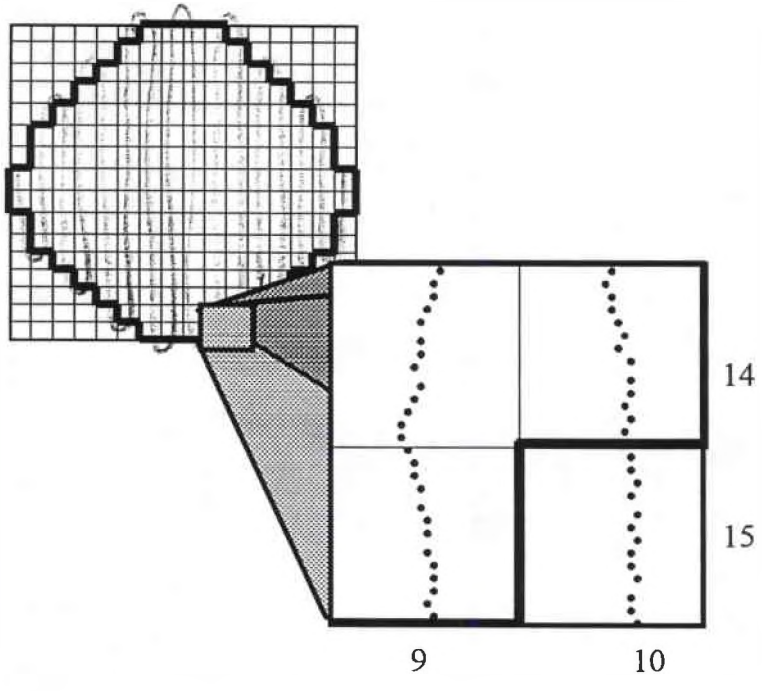

Figure 4 - Notional scan pattern for four pixels

Unfortunately, the pointing accuracy of the sensor limited the ability to collect data for each and every pixel in the telescope field of view. Since the sensor was involved with higher priority collections at the time of this experiment, follow-up scans to fill in gaps in the data were not possible. Knowing this constraint ahead of time, an attempt was made to collect data primarily in the center of the focal plane using several overlapping scans.

Once the data was collected, it was sent, electronically, to the analysis center where it was processed on a Silicon Graphics Indigo™ Workstation. This workstation was equipped with a software package, written in C+ code specifically for this experiment. A listing of the major program source codes are included in Appendix E as a reference.

This software package contains several programs to process the raw data obtained from the sensor into meaningful data values for calibration. The steps performed by the software are outlined below in the order they occur [17].

First a program called "epro2txt" was executed to read in an end product (commonly referred to as "epro") file and generate a text file for each sensor band used in a particular collection file. In most instances, where the filter wheel remained stationary throughout the acquisition of an entire epro data file, only a single file was generated.

Once the epro was successfully read into the software package and converted to understandable and ordered text files, the "fpproc" program was used to process the focal plane data. This program preprocesses the focal

plane data using a two-pass method to remove the linear drift associated with the sensor. This is done by subtracting the value of the first frame as a rough estimate of the DC bias of the detectors. The slope is then calculated by subtracting the pixel value of the first frame from the pixel value of the last frame and then dividing by the number of frames in the text file. Next, to subtract off drift, the program identifies "star pixels" as pixels whose LD value exceeds a stated standard deviation value for a given pixel. This standard deviation may also be raised to decrease the number of false detections or lowered to view dim stars. Following this, the mean and standard deviation are recomputed without star pixels as established by the first pass elimination. A second pass star elimination is then made using this new standard deviation. Finally, a standard linear least squares fit is used to fit the original data with the weights of star pixels set to an effective zero. The standard deviation is recomputed for the corrected data for all pixels and is returned to the "fpproc" program. Figures 5 and 6 below show the effect of this preprocessing algorithm on the collected data. The vertical axis corresponds to measured LDs and the horizontal axis is the frame number.

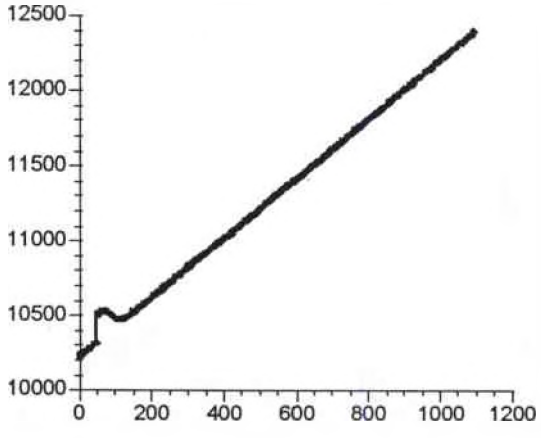

Figure 5 - Plot of raw sensor data

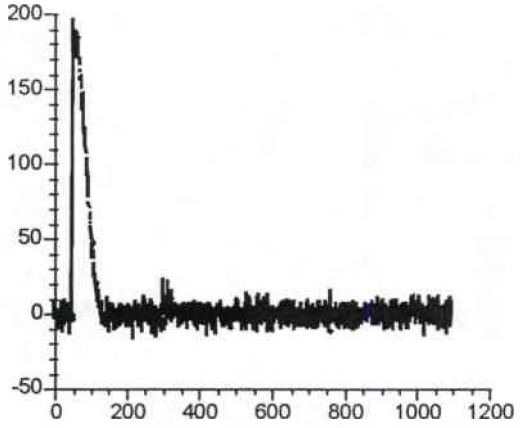

Figure 6 - Plot of preprocessed sensor data

The "fpproc" program also creates several interim files used for this and other types of data analyses. The interim files of interest to this calibration effort include: 1.) highmap.out, 2.) highimap.out, 3.) sdevmap.out, and 4.) highlist.out. The "highmap.out" text file contains N rows by N columns (where N is an integer between zero and 15) of the highest pixel values for each frame number. "Highimap.out" contains the same type of information as highmap.out except the values are now versus frame number are the highest sum-of-nine pixel values. The sum-of-nine value is determined by adding the pixel values of a 3 x 3 grid around the pixel with the maximum LD value for each frame number. "Sdevmap.out" is a N rows by N columns text file of the standard deviation of each pixel over time. Finally, "highlist.out" contains a five column text file with the number of rows equal to the total number of frames in the epro. This file consolidates most of the above data into a single text file containing: 1.) the number of frames, 2.) the X (column) location of the brightest pixel for each frame, 3.) the Y (row) location of the brightest pixel for each frame, 4.) the LD value of the brightest pixel for each frame, and 5.) the sum-of-nine LD values for a pixel grid centered on the brightest pixel for each frame number. These files,

Although these files are used as a basis for further processing, they are available on CD ROM since they are much too large to include on paper.

The information contained in the files mentioned above are used to determine where the star is located on a pixel for a given frame. The method used calculates the "actual" x-y focal plane position for the star for each frame to a predetermined level of accuracy. It begins by first determining the brightest pixel (i.e. pixel with the largest LD value) on the focal plane and then computing a Δx and Δy based on the four surrounding pixel LD values. The graphical depiction of this step is given in Figure 7 below:

P1,3	P2,3	P3,3
P1,2	P2,2	P3,2
P1,1	P2,1	P3,1

Figure 7 - Geometry for centroid calculation

where Δx = P3,2 - P1,2 / (abs(P3,2 - P1,2) + P2,2)

Δy = P2,1 - P2,3 / (abs(P2,1 - P2,3) + P2,2).

The actual x-y position is therefore the sum of the brightest pixel x-y position and the Δx and Δy values, respectively. Specifically, the star's distance from the center of a pixel is determined using the distance formula given as:

$$d = \sqrt{\Delta x^2 + \Delta y^2} \qquad (8)$$

If "d" is less than a previously specified amount of a pixel (i.e. the star is very near the center of the brightest pixel) then the pixel is included in the average calculations. Previous examination of a pixel revealed a nonuniform response

as the star was moved away from its center. Since the difference was substantial, only values of d less than or equal to 0.15 were used for calibration measurements. This is based on a trial and error process of comparing the value of d to the energy measured by the pixel. A point source target such as a star yielded up to an 80 percent loss of energy on the pixel when the star was closer to the outer edge of a given pixel. The resulting average calculations are then stored in the "p2tmp.out" file.

Following these processing steps, matrices of the resulting data values were constructed. These are presented in the form of consolidated pixel LD values for each star in each spectral band and present a clear picture of the focal plane surface and subsequent uniformity. The source for the matrices are the separate processed data files and correspond to each epro file collected. In the interest of report length and understandability, only the consolidated pixel values are included. Appendix H therefore shows the maximum LD value obtained for each pixel on a separate matrix for each star in each band. There is also a matrix on each spreadsheet to report the total number of frames when the star was located near the center of the pixel (i.e. number of measurements which contributed to the average value reported). These numbers provide a "level-of-confidence" for each pixel value and are used to investigate anomalies in the data. The measured LDs are then compared to the predicted LDs for each case and reported in a focal plane matrix (Appendix I) for direct comparison.

CHAPTER IV

OBSERVATIONS AND DATA ANALYSIS

The data collected for this calibration study yielded consistent and accurate data for some stars and sporadic and marginally accurate data for others. The largest differences between the predicted and measured LD values occurred for Lambda Velorum.

The coverage of each star on the focal plane varied considerably depending on the spectral band used and the date of collection. This was primarily due to the pointing error and jitter of the sensor. These independent effects caused unusually low data values for some collections. Combined with data processing timelines and sensor tasking priority, the data coverage was unable to reach 100 percent of the pixels on the focal plane in every band. In addition, a small portion of the values for each collection scenario were less than half of the predicted LD value. It is quite possible this is due to either pixel gap crossing or edge pixel effects.

A simple method was used to analyze the measured LD values reported for each case. The objective was to first obtain a general comparison of the measured and predicted LD values and then assess the accuracy and consistency of the calibration data through error estimation. The general comparison was made by taking the difference between the predicted and measured values for each active pixel was calculated and dividing by the predicted value. The results were displayed as a matrix of decimal values for

each pixel with measured data. A collection of these matrices is included in Appendix I as a reference.

The matrices obtained by the comparison method explained above lead to several general observations for the measurements reported in Appendix H. First, both the consistency (i.e. difference between individual pixel values for a specific collection case) and accuracy (i.e. difference from predicted values) of the measured values are better toward the center of the focal plane than for the outer edge pixels. For example, the accuracy of the pixel values toward the center were between 10 and 20 percent, while the edge pixels varied from 30 to 60 percent. The accuracy of data for both 2 Centauri and Gamma Crucis was approximately 10 to 20 percent for bands 1, 2 , and 3, while it was worse for Alpha Centauri and Lambda Velorum in all bands. The same holds true with respect to the consistency of the measured values. Although the edge pixel values for 2 Centauri and Gamma Crucis were more accurate than those for Alpha Centauri and Lambda Velorum, they were at least 20 percent less accurate than other pixels.

The accuracy of the measured pixel values, assessed in the previous paragraphs, makes no mention of the errors present in the prediction, collection, and data processing methods used in this calibration experiment. Therefore, the next step was to estimate these sources of error in terms of an LD value or overall percentage. If the sum of the error estimates is greater than the difference between the predicted and measured values, the data can be considered useful for absolute calibration.

The calibration of an electro-optical sensor involves the recording and comparison of several measurements against a standard (in this case infrared) source. It is expected that slightly different values would be recorded for each measurement.

The precision of the calibration is important for both reproducibility and consistency reasons while the overall accuracy of the measurements is related to an absolute value. Although neither of these quantities can be measured exactly, due to the physical properties of the sensor, they are addressed here to provide a degree of validity for the absolute values obtained.

One major source of uncertainty in this experiment is the predicted LD values of the star in each spectral band. Reasons for this assessment include: 1) the approximation of stars as a blackbody source, 2) lack of actual spectral measurements and structure within the bandwidth of this sensor, 3) lack of a precise value of the absolute responsivity constant used in the conversion of radiant flux density to LDs for each star, and 4) the assumption of an equal response from all of the pixels on the focal plane array. Engelke reports the approximation of a star's radiant flux density using his function immediately introduces error into the experimental results on the order of 3 to 5 percent [2]. Due to CO_2 and H_2O absorption (primarily in band 3), the spectral structure of each star is not the smooth curve assumed using the blackbody approximation. Fortunately, the fact that the sensor is on-orbit significantly limits this effect since most of the absorption takes place in the earth's atmosphere. However, the lack of actual measurements made above the atmosphere with a spectrometer does limit the degree to which the continuous spectrum between 2.0μm to 3.5μm is known for calibration.

Additionally, the absolute responsivity constant used was determined several years ago in a laboratory prior to deployment of the sensor and is believed to have changed, not only from its initial value, but also between different pixels on the focal plane. Although the approximation of a uniform focal plane array contradicts the results of Vittitoe and George [9], the individual pixel correction factors stated in their report were determined using laboratory data in bands 1 through 4. Regardless, they conclude the pixel to pixel variation to be near 1.4 percent for bands 1, 2, and 3 and as much as 5 percent for band 4. These standard deviations can be used to assess the uniformity of the focal plane but give little insight into the accuracy of each measured value to the predicted value.

Sources of error in this calibration are also present in the actual measurements and data processing. Measurements with this sensor introduce a finite amount of error into the calibration as well. This is primarily a result of physical effects of the sensor optics, such as coma, and electronic effects from the individual detectors. Although the star is considered a point source, as received at the telescope aperture, the telescope optics cause the image to spread over a finite distance (typically smaller than the size of a single pixel). However, this spot size tends to increase toward the outer edges of the field of view of the sensor. The result is a directionally dependent spreading of the source energy and the 3 x 3 centroid calculation may not be the ideal shape to capture the entire signal. An error estimate must therefore be included in the final analysis to account for this phenomenon. In the center of the focal plane array, this effect is minimal at less than one half of one percent of the total LD

value. However, on the edge pixels, this effect can increase the error to 10 percent.

The data processing contributes to error in the results of this calibration as well. Factors such as the linear estimation and subsequent removal of the sensor's thermal drift and the proper calculation and removal of the background signal can substantially impact the reported star measurements for all cases. Examination of the linear drift removal indicates an error of nearly 5 LDs for a signal of 200 LDs. This error estimate of 2.5 percent assumes the drift is indeed linear and thus an accurate modeling and removal of this effect is done. In cases where the drift is nonlinear the error increases considerably and can lead to very large or small LD values (more than 100 percent from predicted values) for specific pixels or cases. As a result, they can be easily identified, located, and discarded as valid data if necessary.

The background noise is due primarily to the background radiation of space and the detector noise. A calculation of the signal-to-noise ratio therefore aids in the determination of a viable error estimate for this effect. Although the processing software effectively removed the background noise from the signal, a DC signal of up to 10 LDs remained for a signal strength of nearly 200 LDs. This, in turn, caused the final reported signal to deviate from the expected LD value by as much as 5 percent.

Consolidating all the error estimates mentioned above leads to an acceptable error of nearly 20 percent for this method of calibration. This estimate pertains to pixels not located on the edge of the field of view. Since most of the errors influencing the measured results are more prominent near the

edge pixels, the 20 percent estimate is not sufficient and specific factors such as coma and sum-of-nine processing with inactive pixels must be investigated further in the future.

The results for both 2 Centauri and Gamma Crucis appear to fall within this error estimate for most cases. The band 4 data for 2 Centauri is much lower than predicted and may be a result of the detector material cutoff wavelength mentioned earlier. Alpha Centauri contains accurate data for band 1 but not bands 2 and 3. However, the edge pixel differences from the center pixel values are not as prominent for this star. It is possible that the lack of consistency in measurements for this star are the result of a processing error (such as the linear approximation and removal of thermal drift) rather than a physical phenomenon or theoretical prediction error.

CHAPTER V

CONCLUSIONS

The accuracy of the calibration results were highly dependent on both the prediction method and the characterization and subtraction of the sensor noise effects. The most accurate method (currently available) was chosen for this calibration study. A straightforward and logical path was chosen for both the star selection and data processing to make the experiment easily repeatable for future re-calibrations of this and other similar sensors.

In general the data obtained for 2 Centauri and Gamma Crucis in bands 1, 2, and 3 can be used to make a meaningful assessment of the accuracy of the current responsivity constant for the sensor. It is determined that this constant has not changed more than the error boundary (within 10 percent of the expected value) of this calibration. However, a sufficient amount of data was not obtained to make an accurate assessment of the responsivity constant for individual pixels, including those on the outer edges of the focal plane array. Data collected for Alpha Centauri, Lambda Velorum, and all of band 4 supports these conclusions for some cases but contain random and systematic errors deviations which require further investigation.

The zeroing out of the edge pixel LD values appears to affect the results. In a majority of the matrices of collected data in Appendix H, the edge pixels contain either a zero value or one well below the predicted LD value. This may be due to the onboard processing of the data that zeroes the LD value of pixels

outside of the sensor's field of view. Thus, any star energy on these pixels, when adjacent to a target pixel is lost for the sum-of-nine calculation. Another possible effect is coma [18]. The telescope of the sensor, though not characterized precisely, is known to have coma. As a result, it is possible the energy is spread out among more than the nine pixels used in the LD calculation. This optical effect would be most prominent along the outer edges of the focal plane array. The energy could also be spread unevenly at these locations whereby it covers nine pixels in a rectangular shape rather than the 3 x 3 square used in this experiment.

The errors in this experiment, for the majority of cases, are concluded to be systematic rather than random. This is based on the observation that the central pixels on the focal plane were typically within 10 percent of their predicted values for most cases. More specifically, the focal plane uniformity was found to be consistent within 5 percent for several cases and near the center of the focal plane array. 2 Centauri, Gamma Crucis, and Lambda Velorum yielded particularly good results in bands 1 and 2, while Alpha Centauri and all band 3 and 4 measurements were slightly worse. These non-uniformities may have resulted from either the data processing technique (e.g. treatment of the edge pixels) or coma. Although some degree of nonuniformity across the focal plane array is expected, it is unlikely the variation is greater than 5-10 LDs for pixels not located near the edge of the field of view. On edge pixels, where the difference is greater than 10 LDs, the deviation is more likely a result of either coma or inactive pixels as part of the centroid calculation. Although the effect of coma is not known on a pixel-by-pixel basis, it would be valuable to investigate this in greater detail in future work with this sensor. However, indications of coma from the telescope optics do seem to be present despite the limited

amount of data collected. This effect must be characterized further before an accurate assessment and subsequent correction of the edge pixel values is made.

Due to limited availability of the sensor for acquiring calibration data, the band 4 collections were constrained to only 2 Centauri and Lambda Velorum. Ambiguities are present in this band and are expected to be a result of the cutoff wavelength being very near to the HgCdTe material used for the focal plane, Large errors with Lambda Velorum in band 4 (and the other 3 bands) may also have occurred from the author's calculation of Ω, since the well characterized and more accurate Engelke value was not available for this star. It is recommended that future calibrations with this star, and others not cited in the Engelke report, involve a more rigorous approach for calculating Ω than the one outlined in Appendix C of this report. Although the accuracy of the theoretical predictions for Lambda Velorum are not useful for absolute calibration, the consistency of the measured values indicates that the star is a promising candidate for future re-calibration of this sensor or focal plane uniformity and gap correction studies.

Recommendations for future calibrations of this sensor focus on the improved accuracy of the star radiance predictions and corresponding LD values. Although the Engelke Function was the most comprehensive prediction tool available at the time of this report, increased low resolution measurements and expanded databases of continuous star radiances in the short wave infrared, may produce smaller margins of error in future experiments. The additional data could also be used as a basis for predicting the LD values of the candidate stars. This will eliminate the need for blackbody approximations and

increase the overall accuracy of the predicted LD values for each case. Furthermore, the increased accuracy of the prediction values could be used to determine the amount of energy lost when the center of a star (or other point source target) crosses a pixel gap or falls on an edge pixel. Although the actual size of the pixel gap is an order of magnitude smaller than the size of a pixel, it is known to have a measureable affect on other collections made with this sensor. Whether pixel gap crossings significantly alter the values obtained for star calibration is not yet determined.

It is also recommended that data collections, spread out over the course of a year and reevaluated annually, should be used to characterize the variance in the LD values per pixel, both over time and in response to seasonal changes in focal plane temperature and viewing geometry.

APPENDIX A

SENSOR DESCRIPTION [19]

The sensor used in this calibration effort was custom built in 1989. It contains a 256 element HgCdTe focal plane array and has approximately a quarter degree field of view. Each pixel is welded to one element of a 16 x 16 silicon CCD charge storage and multiplexer array. The multiplexer is composed of 16 parallel 16 stage CCD arrays that empty into a single element of a 16 stage readout array. A charge amplifier then converts the output of the readout array to a proportional voltage of 2.334×10^{-7} volts/electron. This voltage represents the charge from each pixel on the focal plane. The multiplexer array is driven by a 100 kHz gated four phase clock. This clock drives the sixteen stage serial output array. The CCD serial output array shifts a total of 16 times, corresponding to a pixel's value each shift. This process is repeated 16 times to complete the total 256 pixel readout cycle. The total time required for the array readout cycle is 3.0797 milliseconds.

The focal plane array's temperature is controlled with a thermoelectric cooler. This device allows the sensor temperature to be controlled to within $0.01^{o}C$ and minimizes sensor noise caused by low frequency temperature variations. The sensor temperature is held between $150^{0}K$ and $170^{0}K$ depending on season.

The optical system includes a three element ZnSe imaging system and a six position filter wheel. The six filters are each located 60 degrees apart from one another. This instrument enables one of five specific infrared bands to be transmitted to the sensor. The fifth filter is a wide open band and covers the entire operating range of the focal plane while the sixth filter position contains an opaque gold foil and is used to protect the sensor from accidentally viewing the sun while the telescope is being stowed. A stepper motor is used to rotate the filter wheel when desired. It is able to move between adjacent filters in 202 milliseconds and can rotate between filters up to 180 degrees apart in 406 milliseconds.

The sensor's data processor digitizes the serial CCD output and sums and sums a variable number (1-63 cycles/frame) of the unique pixel values. This generates a nominal 0.1 second 18 bit sum for each pixel and is referred to as a single data frame. The data frames are then either passed to the extended memory location or downlinked to a ground processor at a rate of 32,000 bits per second.

APPENDIX B

BLACKBODY APPROXIMATION FOR STARS

This calibration study assumes the radiation from each star used has a spectral distribution that closely resembles a blackbody. This approximation is based on the data presented in *The Infrared and Electro-Optical Systems Handbook* [10], and other published works.

The most significant deviations from a blackbody occur when a star is viewed from a ground based sensor. Propagation of the star's radiation is thus subjected to both attenuation and absorption due to elements in the earth's atmosphere such as carbon dioxide and water. Absorption bands in the 2.0μm to 3.5μm region for CO_2 and H_20 can substantially lower the amount of radiation reaching the sensor and produce inaccurate measurements. Since the sensor investigated here is positioned in orbit above the atmosphere, these affects are negligible, leading to increased validity of the blackbody approximation.

Ramsey [20] compares the irradiance from the sun, as measured above the atmosphere, with standard blackbody curves of 5700^{0}K and 6000^{0}K. This plot shows no measurable difference between the shape of the three curves in the 2.0μm to 3.5μm region except for specific spectral lines at specified wavelengths. The bandwidth of these spectral lines is, in most cases considerably more narrow than the resolution of the bandwidth of the individual sensor filters. Since Alpha Centauri is the same spectral class as the sun, its

approximation as a blackbody source is reasonably accurate for this level of calibration.

Engelke [1,2], on the other hand, compares a computer generated function based on Planckian distribution to actual measured values at specific wavelengths. Therefore, he also states the stars used to verify his function approximate a blackbody in the region from 2μm to 60μm. The report also includes deviations of no more than three percent over the operating wavelength of this sensor [2]. Published error values such as these support the assumption that the stars chosen for this calibration resemble a blackbody spectral distribution.

APPENDIX C

Ω CALCULATION FOR LAMBDA VELORUM

Since the Engelke Report does not include a value of the angular size of the star Lambda Velorum, this value was approximated using MathCad®. In order to accomplish this, published magnitude values from *NASA's Catalog of Infrared Observations* [21] were used from 2.2μm and 3.5μm. These values were then converted to radiant flux units of W/cm^2/μm using the data contained in Table 2.1 of this report [10]. A summary of the calculation is included below:

Given: $\lambda = 2.2\mu m$, $T_e = 3800$, $E = 2.81 \times 10^{-12}$ W/cm^2

$$T = 0.738\lambda T_e\left(1+\frac{79450}{\lambda T_e}\right)^{0.182}$$

$$\Omega_{2.2} = E\lambda^5\left[\frac{\exp\left(\frac{14388}{\lambda T}\right)-1}{11910}\right]$$

$$\Omega_{2.2} = 1.211\times 10^{-14}\,\text{sr}$$

Given: $\lambda = 3.5\mu m$, $T_e = 3800$, $E = 6.19 \times 10^{-13}$ W/cm^2

$$T = 0.738\lambda T_e\left(1+\frac{79450}{\lambda T_e}\right)^{0.182}$$

$$\Omega_{3.5} = E\lambda^5\left[\frac{\exp\left(\frac{14388}{\lambda T}\right)-1}{11910}\right]$$

$$\Omega_{3.5} = 9.334\times 10^{-15}\,\text{sr}$$

Using the values obtained above a simple average is taken to approximate the angular size of Lambda Velorum in the spectral region of this sensor.

$$\Omega = \frac{\Omega_{2.2}+\Omega_{3.5}}{2}$$

$$\Omega = 1.072\times 10^{-14}\,\text{sr}$$

APPENDIX D

COLLECTION FILES USED FOR CALIBRATION [22]

EPRO File	Star	Date Collected	Filter Wheel
011487184	2 Centauri	21 Oct 95	1
011487187	2 Centauri	21 Oct 95	1
011487197	2 Centauri	22 Oct 95	1
011487198	2 Centauri	22 Oct 95	1
011487192	2 Centauri	22 Oct 95	2
011487194	2 Centauri	22 Oct 95	2
011532806	2 Centauri	29 Oct 95	3
011532807	2 Centauri	29 Oct 95	3
011472445	2 Centauri	19 Oct 95	4
011472446	2 Centauri	19 Oct 95	4
011472453	2 Centauri	20 Oct 95	4
011472454	2 Centauri	20 Oct 95	4
011472455	2 Centauri	20 Oct 95	4
011472456	2 Centauri	20 Oct 95	4
011487178	2 Centauri	21 Oct 95	4
011487179	2 Centauri	21 Oct 95	4
011976978	Alpha Centauri	14 Jan 96	1
011976980	Alpha Centauri	14 Jan 96	1
011976981	Alpha Centauri	14 Jan 96	1
011976982	Alpha Centauri	14 Jan 96	2
011976983	Alpha Centauri	14 Jan 96	2
011981574	Alpha Centauri	14 Jan 96	2
011976984	Alpha Centauri	14 Jan 96	3
011976985	Alpha Centauri	14 Jan 96	3
011976986	Alpha Centauri	14 Jan 96	3

EPRO File	Star	Date Collected	Filter Wheel
011976987	Gamma Crucis	15 Jan 96	1
011976988	Gamma Crucis	15 Jan 96	1
011976989	Gamma Crucis	15 Jan 96	1
011976990	Gamma Crucis	15 Jan 96	1
011976995	Gamma Crucis	15 Jan 96	2
011977044	Gamma Crucis	15 Jan 96	2
011977045	Gamma Crucis	15 Jan 96	2
011998997	Gamma Crucis	15 Jan 96	3
011998998	Gamma Crucis	15 Jan 96	3
011998999	Gamma Crucis	15 Jan 96	3
011999000	Gamma Crucis	15 Jan 96	3
011678231	Lambda Velorum	15 Nov 95	1
011682191	Lambda Velorum	15 Nov 95	1
011687768	Lambda Velorum	15 Nov 95	1
011707051	Lambda Velorum	16 Nov 95	2
011707052	Lambda Velorum	16 Nov 95	2
011707053	Lambda Velorum	16 Nov 95	2
011707054	Lambda Velorum	16 Nov 95	2
011707055	Lambda Velorum	17 Nov 95	3
011707123	Lambda Velorum	17 Nov 95	3
011707124	Lambda Velorum	17 Nov 95	3
011709037	Lambda Velorum	18 Nov 95	4
011709336	Lambda Velorum	18 Nov 95	4
011710061	Lambda Velorum	18 Nov 95	4

APPENDIX E

PROCESSING PROGRAM SOURCE CODE [24]

FPSIM Program Source Code

```
#include <stdio.h>
#include <stdlib.h>
#include <math.h>
#ifdef MAC
#define M_PI _PI
#define M_PI_2 _PI/2.0
#endif
#define ARRAY_SIZE 15
#define NFRAMES 1100
#define TSTART  50
#define TFRAMES 1000
#define NOISE 5.0
#define YNOISE 0.1
#define TARGET 200.0

double gaussrand();
double errfc();
void nrerror();

void main(int argc, char *argv[])
{
  int xdim,ydim,xdex,ydex,framedex,kdex,idex,jdex,npix;
  double *txpos,*typos,toffset,tslope;
  float *frames,***data;

  double c1,cx,cy,xdelta,ydelta,xarg1,xarg2,yarg1,yarg2,ktmp;

      FILE *fpdata;

  if (argc==2)
    xdim=ydim=atoi(argv[1]);
  else if (argc==3)
    {
      xdim=atoi(argv[1]);
      ydim=atoi(argv[2]);
    }
  else
    xdim=ydim=ARRAY_SIZE;

  if ((txpos=(double *)calloc(TFRAMES,sizeof(double)))==NULL)
      nrerror("Calloc error on txpos");
```

```
 if ((typos=(double *)calloc(TFRAMES,sizeof(double)))==NULL)
     nrerror("Calloc error on typos");
 if ((frames=(float *)calloc(NFRAMES,sizeof(float)))==NULL)
     nrerror("Calloc error on frames");

 if ((data=(float ***)calloc(ydim,sizeof(float **)))==NULL)
     nrerror("Calloc error");
 for (ydex=0;ydex<ydim;ydex++)
     {
        if ((data[ydex]=(float **)calloc(xdim,sizeof(float *)))==NULL)
                nrerror("Calloc error");
    for (xdex=0;xdex<xdim;xdex++)
                        if ((data[ydex][xdex]=(float *)calloc(NFRAMES,sizeof(float)))==NULL)
                        nrerror("Calloc error");
        }
     /* Create background */
     for (framedex=0;framedex<NFRAMES;framedex++)
        frames[framedex]=(float)framedex;
     for (ydex=0;ydex<ydim;ydex++)
     for (xdex=0;xdex<ydim;xdex++)
     {
        toffset=10000.0+500*gaussrand();
        tslope=1.0+gaussrand();
                        for (framedex=0;framedex<NFRAMES;framedex++)
                data[ydex][xdex][framedex]=toffset+(float)framedex*tslope+gaussrand()*NOISE;
                }
     /* Add target */
 for (framedex=0;framedex<TFRAMES;framedex++)
  {
    txpos[framedex]=fabs(fmod((double)(xdim-
1)*(double)ydim*(double)framedex/(double)TFRAMES,(double)(xdim-1)));

typos[framedex]=floor((double)ydim*(double)framedex/(double)TFRAMES)+YNOISE*gaussrand(
);
    c1=M_PI_2/0.5;
    cx=0.5*c1;
    cy=0.5*c1;
    for (ydex=0;ydex<ydim;ydex++)
                        for (xdex=0;xdex<xdim;xdex++)
                        {
                           xdelta=txpos[framedex]-(double)xdex;
                           ydelta=typos[framedex]-(double)ydex;
                        xarg1=fabs(c1*xdelta);
                           xarg2=xarg1-cx;
                           yarg1=fabs(c1*ydelta);
                           yarg2=yarg1-cy;
                           ktmp=0.25*
                             (errfc(xarg2)-errfc(xarg1+cx))*
                             (errfc(yarg2)-errfc(yarg1+cy));
                         data[ydex][xdex][TSTART+framedex]+=ktmp*TARGET;
                        }
  }
 /* Make data file */
     if ((fpdata=fopen("rawfp.txt","w"))==NULL)
        nrerror("Error opening array.out");
 for (framedex=0;framedex<NFRAMES;framedex++)
```

```
  {
  fprintf(fpdata,"%5d ",framedex);
    for (ydex=0;ydex<ydim;ydex++)
                              for (xdex=0;xdex<ydim;xdex++)
                                fprintf(fpdata,"%.0lf ",data[ydex][xdex][framedex]);
      fprintf(fpdata,"\n");
  }
fclose(fpdata);

      /* Dump real trajectories */
      if ((fpdata=fopen("rawtraj.out","w"))==NULL)
          nrerror("Error opening traj.out");
      for (framedex=0;framedex<TFRAMES;framedex++)
      fprintf(fpdata,"%f %f\n",txpos[framedex],typos[framedex]);
      fclose(fpdata);
}
```

FPPROC Program Source Code

```
#include <stdio.h>
#include <stdlib.h>
#include <string.h>
#include <math.h>
/* #define DEBUG */
/* #define MAC */
#ifdef MAC
#define M_PI _PI
#define M_PI_2 _PI/2.0
#endif
#define THRESH 3.0
#define NCRIT 5
#define NCRIT2 3

void nrerror();
float preprocess();
void fit();

void main(int argc, char *argv[])
{
  char fname[200], lbuff[5002];
  const char toksep[2]=" \000";
  FILE *fp_infile;
  int xdim,ydim,xdex,ydex,framedex,kdex,idex,jdex,npix,NFRAMES=0,npixels=0;
  int ***target;
  float
*frames,***data,***data1,***totali,**highmap,**highimap,**sdevmap,*highpix,*highsum,*highpofm
ax,*highipofmax,*rtx,*rty;
  int *highx,*highy;

  float crit[NCRIT] ={ 0.85,0.90,0.95,0.97,0.99 };
  float ***critave;
  int ***critn,critdex=0;

  float crit2[NCRIT2] ={ 0.20,0.10,0.15 };
  float ***crit2ave;
  int ***crit2n;

  int rtxi,rtyi;
  float rtxf,rtyf;

  FILE *fpdata;

  double c1,cx,cy,xdelta,ydelta,xarg1,xarg2,yarg1,yarg2,ktmp;

  int pixhighx,pixhighy;
  double pixhigh,deltax,deltay;

#ifdef MAC
  sprintf(fname,"rawfp.txt");
#else
  if (argc!=2)
    nrerror("usage: fpproc filename");
```

```
  sprintf(fname,"%s",argv[1]);
#endif

  if ((fp_infile=fopen(fname,"r"))==NULL)
    nrerror("Error opening file");

  while (fgets(lbuff,5000,fp_infile)!=NULL)
    NFRAMES++;

  rewind(fp_infile);
  fgets(lbuff,5000,fp_infile);
  strtok(lbuff,toksep);
  while (strtok(NULL,toksep)!=NULL)
    npixels++;
  npixels--;
  xdim=ydim=(int)sqrt((float)npixels);
  rewind(fp_infile);

  if ((data=(float ***)calloc(ydim,sizeof(float **)))==NULL)
    nrerror("Calloc error");
  if ((data1=(float ***)calloc(ydim,sizeof(float **)))==NULL)
    nrerror("Calloc error");
  if ((totali=(float ***)calloc(ydim,sizeof(float **)))==NULL)
    nrerror("Calloc error");
  if ((highmap=(float **)calloc(ydim,sizeof(float *)))==NULL)
    nrerror("Calloc error");
  if ((highimap=(float **)calloc(ydim,sizeof(float *)))==NULL)
    nrerror("Calloc error");
  if ((sdevmap=(float **)calloc(ydim,sizeof(float *)))==NULL)
    nrerror("Calloc error");
  if ((frames=(float *)calloc(NFRAMES,sizeof(float)))==NULL)
    nrerror("Calloc error");
  if ((highx=(int *)calloc(NFRAMES,sizeof(int)))==NULL)
    nrerror("Calloc error");
  if ((highy=(int *)calloc(NFRAMES,sizeof(int)))==NULL)
    nrerror("Calloc error");
  if ((highpix=(float *)calloc(NFRAMES,sizeof(float)))==NULL)
    nrerror("Calloc error");
  if ((highsum=(float *)calloc(NFRAMES,sizeof(float)))==NULL)
    nrerror("Calloc error");
  if ((highpofmax=(float *)calloc(NFRAMES,sizeof(float)))==NULL)
    nrerror("Calloc error");
  if ((highipofmax=(float *)calloc(NFRAMES,sizeof(float)))==NULL)
    nrerror("Calloc error");
  if ((rtx=(float *)calloc(NFRAMES,sizeof(float)))==NULL)
    nrerror("Calloc error");
  if ((rty=(float *)calloc(NFRAMES,sizeof(float)))==NULL)
    nrerror("Calloc error");
  if ((critn=(int ***)calloc(ydim,sizeof(int **)))==NULL)
    nrerror("Calloc error");
  if ((critave=(float ***)calloc(ydim,sizeof(float **)))==NULL)
    nrerror("Calloc error");
  if ((crit2n=(int ***)calloc(ydim,sizeof(int **)))==NULL)
    nrerror("Calloc error");
  if ((crit2ave=(float ***)calloc(ydim,sizeof(float **)))==NULL)
    nrerror("Calloc error");
```

```
if ((target=(int ***)calloc(ydim,sizeof(int **)))==NULL)
  nrerror("Calloc error");
for (ydex=0;ydex<ydim;ydex++)
 {
   if ((data[ydex]=(float **)calloc(xdim,sizeof(float *)))==NULL)
     nrerror("Calloc error");
   if ((data1[ydex]=(float **)calloc(xdim,sizeof(float *)))==NULL)
     nrerror("Calloc error");
   if ((totali[ydex]=(float **)calloc(xdim,sizeof(float *)))==NULL)
     nrerror("Calloc error");
   if ((highmap[ydex]=(float *)calloc(xdim,sizeof(float)))==NULL)
     nrerror("Calloc error");
   if ((highimap[ydex]=(float *)calloc(xdim,sizeof(float)))==NULL)
     nrerror("Calloc error");
   if ((sdevmap[ydex]=(float *)calloc(xdim,sizeof(float)))==NULL)
     nrerror("Calloc error");
   if ((critn[ydex]=(int **)calloc(xdim,sizeof(int *)))==NULL)
     nrerror("Calloc error");
   if ((critave[ydex]=(float **)calloc(xdim,sizeof(float *)))==NULL)
     nrerror("Calloc error");
   if ((crit2n[ydex]=(int **)calloc(xdim,sizeof(int *)))==NULL)
     nrerror("Calloc error");
   if ((crit2ave[ydex]=(float **)calloc(xdim,sizeof(float *)))==NULL)
     nrerror("Calloc error");
   if ((target[ydex]=(int **)calloc(xdim,sizeof(int *)))==NULL)
     nrerror("Calloc error");
   for (xdex=0;xdex<xdim;xdex++)
     {
       if ((data[ydex][xdex]=(float *)calloc(NFRAMES,sizeof(float)))==NULL)
         nrerror("Calloc error");
       if ((data1[ydex][xdex]=(float *)calloc(NFRAMES,sizeof(float)))==NULL)
         nrerror("Calloc error");
       if ((totali[ydex][xdex]=(float *)calloc(NFRAMES,sizeof(float)))==NULL)
         nrerror("Calloc error");
       if ((target[ydex][xdex]=(int *)calloc(NFRAMES,sizeof(int)))==NULL)
         nrerror("Calloc error");
       if ((critn[ydex][xdex]=(int *)calloc(NCRIT,sizeof(int)))==NULL)
         nrerror("Çalloc error");
       if ((critave[ydex][xdex]=(float *)calloc(NCRIT,sizeof(float)))==NULL)
         nrerror("Calloc error");
       if ((crit2n[ydex][xdex]=(int *)calloc(NCRIT2,sizeof(int)))==NULL)
         nrerror("Çalloc error");
       if ((crit2ave[ydex][xdex]=(float *)calloc(NCRIT2,sizeof(float)))==NULL)
         nrerror("Calloc error");
     }
 }
/* Read data */

for (framedex=0;framedex<NFRAMES;framedex++)
 {
   if (fgets(lbuff,5000,fp_infile)==NULL)
     nrerror("Error reading file");
   frames[framedex]=atof(strtok(lbuff,toksep));
   for (ydex=0;ydex<ydim;ydex++)
     for (xdex=0;xdex<xdim;xdex++)
       data[ydex][xdex][framedex]=atof(strtok(NULL,toksep));
```

```
  }
 /* Dump original array */
 if ((fpdata=fopen("array.out","w"))==NULL)
  nrerror("Error opening array.out");
 for (framedex=0;framedex<NFRAMES;framedex++)
  {
   fprintf(fpdata,"%5.0f ",frames[framedex]);

#ifdef DEBUG
    for (ydex=0;ydex<ydim;ydex++)
     for (xdex=0;xdex<xdim;xdex++)
#else
    ydex=xdex=8;
#endif
      fprintf(fpdata,"%.0lf ",data[ydex][xdex][framedex]);
    fprintf(fpdata,"\n");
  }
 fclose(fpdata);

 /* Preprocess */
 for (ydex=0;ydex<ydim;ydex++)
  for (xdex=0;xdex<xdim;xdex++)
   {
   fprintf(stderr,"X: %d Y: %d    ",xdex,ydex);

sdevmap[ydex][xdex]=preprocess(frames,data[ydex][xdex],data1[ydex][xdex],NFRAMES,target[
ydex][xdex]);
    }
 /* Dump preprocessed array */
 if ((fpdata=fopen("parray.out","w"))==NULL)
  nrerror("Error opening array.out");
 for (framedex=0;framedex<NFRAMES;framedex++)
  {
   fprintf(fpdata,"%5d ",framedex);
#ifdef DEBUG
    for (ydex=0;ydex<ydim;ydex++)
     for (xdex=0;xdex<xdim;xdex++)
#else
    ydex=xdex=8;

#endif
      fprintf(fpdata,"%6.2lf ",data1[ydex][xdex][framedex]);
    fprintf(fpdata,"\n");
  }
 fclose(fpdata);

 /* Load High Map */
 for (ydex=0;ydex<ydim;ydex++)
  for (xdex=0;xdex<xdim;xdex++)
   {
highmap[ydex][xdex]=data1[ydex][xdex][0];
    for (framedex=0;framedex<NFRAMES;framedex++)
     if (highmap[ydex][xdex]<data1[ydex][xdex][framedex])
      highmap[ydex][xdex]=data1[ydex][xdex][framedex];
   }
 /* Fill totali array with 25 pixel sum */
```

```
#define KNUM 2

for (framedex=0;framedex<NFRAMES;framedex++)
  for (ydex=0;ydex<ydim;ydex++)
    for (xdex=0;xdex<xdim;xdex++)
      for (jdex=ydex-KNUM;jdex<=ydex+KNUM;jdex++)
        for (idex=xdex-KNUM;idex<=xdex+KNUM;idex++)
          if (jdex>-1 && jdex<ydim && idex>-1 && idex<xdim)
            totali[ydex][xdex][framedex]+=data1[jdex][idex][framedex];

/* Load totali High Map */
for (ydex=0;ydex<ydim;ydex++)
  for (xdex=0;xdex<xdim;xdex++)
    {
      highimap[ydex][xdex]=totali[ydex][xdex][0];
      for (framedex=0;framedex<NFRAMES;framedex++)
        if (highimap[ydex][xdex]<totali[ydex][xdex][framedex])
          highimap[ydex][xdex]=totali[ydex][xdex][framedex];
    }
/* Load High List */
for (framedex=0;framedex<NFRAMES;framedex++)
  {
    highx[framedex]=highy[framedex]=0;
    highpix[framedex]=data1[0][0][framedex];
    highpofmax[framedex]=data1[0][0][framedex]/highmap[0][0];
    highipofmax[framedex]=totali[0][0][framedex]/highimap[0][0];
    highsum[framedex]=totali[0][0][framedex];
    for (ydex=0;ydex<ydim;ydex++)
      for (xdex=0;xdex<xdim;xdex++)
        if (highpix[framedex]<data1[ydex][xdex][framedex])
          {
            highx[framedex]=xdex;
            highy[framedex]=ydex;
            highpix[framedex]=data1[ydex][xdex][framedex];
          }
    ydex=highy[framedex];
    xdex=highx[framedex];

    highsum[framedex]=totali[ydex][xdex][framedex];
    highpofmax[framedex]=data1[ydex][xdex][framedex]/highmap[ydex][xdex];
    highipofmax[framedex]=totali[ydex][xdex][framedex]/highimap[ydex][xdex];

    rtx[framedex]=(float)highx[framedex];
    rty[framedex]=(float)highy[framedex];

    if (ydex>0 && ydex<(ydim-1))
      rty[framedex]+=(data1[ydex+1][xdex][framedex]-data1[ydex-1][xdex][framedex])/
      (fabs((data1[ydex+1][xdex][framedex]-data1[ydex-
1][xdex][framedex]))+fabs(data1[ydex][xdex][framedex]));
    else
      rty[framedex]=-rty[framedex];
    if (xdex>0 && xdex<(xdim-1))
      rtx[framedex]+=(data1[ydex][xdex+1][framedex]-data1[ydex][xdex-1][framedex])/
      (fabs((data1[ydex][xdex+1][framedex]-data1[ydex][xdex-
1][framedex]))+fabs(data1[ydex][xdex][framedex]));
    else
```

```
      rtx[framedex]=-rtx[framedex];

    if (fabs(highpix[framedex])<THRESH*sdevmap[ydex][xdex] &&
target[ydex][xdex][framedex])
      {
        highx[framedex]=-highx[framedex]-1;
        highy[framedex]=-highy[framedex]-1;
        rty[framedex]=-rty[framedex];
        rtx[framedex]=-rtx[framedex];
      }
   }
  /* Dump highmap */
  if ((fpdata=fopen("highmap.out","w"))==NULL)
    nrerror("Error opening highmap.out");
  for (ydex=0;ydex<ydim;ydex++)
   {
     for (xdex=0;xdex<xdim;xdex++)
       fprintf(fpdata,"%6.2lf ",highmap[ydex][xdex]);
     fprintf(fpdata,"\n");
   }
  fclose(fpdata);

  /* Dump totali highmap */
  if ((fpdata=fopen("highimap.out","w"))==NULL)
    nrerror("Error opening highimap.out");
  for (ydex=0;ydex<ydim;ydex++)
   {
     for (xdex=0;xdex<xdim;xdex++)
       fprintf(fpdata,"%6.2lf ",highimap[ydex][xdex]);
     fprintf(fpdata,"\n");
   }
  fclose(fpdata);

  /* Dump sdevmap */
  if ((fpdata=fopen("sdevmap.out","w"))==NULL)
    nrerror("Error opening highimap.out");
  for (ydex=0;ydex<ydim;ydex++)
   {
     for (xdex=0;xdex<xdim;xdex++)
       fprintf(fpdata,"%6.2lf ",sdevmap[ydex][xdex]);
     fprintf(fpdata,"\n");
   }
  fclose(fpdata);

  /* Dump High List */
  if ((fpdata=fopen("highlist.out","w"))==NULL)
    nrerror("Error opening highlist.out");
  for (framedex=0;framedex<NFRAMES;framedex++)
    fprintf(fpdata,"%f %d %d %f
%f\n",frames[framedex],highx[framedex],highy[framedex],highpix[framedex],highsum[framedex]
);
  fclose(fpdata);

  /* Dump processed array */
  if ((fpdata=fopen("pparray.out","w"))==NULL)
    nrerror("Error opening array.out");
```

```
  for (framedex=0;framedex<NFRAMES;framedex++)
    {
      fprintf(fpdata,"%5d ",framedex);
#ifdef DEBUG
      for (ydex=0;ydex<ydim;ydex++)
        for (xdex=0;xdex<xdim;xdex++)
#else
      ydex=xdex=5;
#endif
          fprintf(fpdata,"%6.2lf ",totali[ydex][xdex][framedex]);
      fprintf(fpdata,"\n");
    }
  fclose(fpdata);

  /* Dump some info for development */
  if ((fpdata=fopen("tmp.out","w"))==NULL)
    nrerror("Error opening traj.out");
  for (framedex=0;framedex<NFRAMES;framedex++)
    fprintf(fpdata,"%5d %6.4f %6.4f %7.2f %7.2f %6.4f %6.4f\n",framedex,

rtx[framedex],rty[framedex],highpix[framedex],highsum[framedex],highpofmax[framedex],highip
ofmax[framedex]);
  fclose(fpdata);

  /* Criteria process */

  if ((fpdata=fopen("p1tmp.out","w"))==NULL)
    nrerror("Error opening traj.out");

  for (ydex=0;ydex<ydim;ydex++)
    for (xdex=0;xdex<xdim;xdex++)
      {
        critn[ydex][xdex][critdex]=0;
        critave[ydex][xdex][critdex]=0.0;
        fprintf(fpdata,"%4d   ",ydex*xdim+xdex);
        for (critdex=0;critdex<NCRIT;critdex++)
          {
            for (framedex=0;framedex<NFRAMES;framedex++)
              if (data1[ydex][xdex][framedex]>crit[critdex]*highmap[ydex][xdex] &&
target[ydex][xdex][framedex])
              {
                critave[ydex][xdex][critdex]+=totali[ydex][xdex][framedex];
                critn[ydex][xdex][critdex]++;
              }
            if (critn[ydex][xdex][critdex]!=0.0)
              critave[ydex][xdex][critdex]/=critn[ydex][xdex][critdex];
            else
              critave[ydex][xdex][critdex]=0.0;
            fprintf(fpdata,"%8.2f %6d  ",critave[ydex][xdex][critdex],critn[ydex][xdex][critdex]);
          }
        fprintf(fpdata,"\n");
      }
  if ((fpdata=fopen("p1atmp.out","w"))==NULL)
    nrerror("Error opening traj.out");

  for (ydex=0;ydex<ydim;ydex++)
```

```
 {
  for (xdex=0;xdex<xdim;xdex++)
   fprintf(fpdata,"%8.2f ",critave[ydex][xdex][0]);
  fprintf(fpdata,"\n");
 }
fprintf(fpdata,"\n");
for (ydex=0;ydex<ydim;ydex++)
 {
  for (xdex=0;xdex<xdim;xdex++)
   fprintf(fpdata,"%8d ",critn[ydex][xdex][0]);
  fprintf(fpdata,"\n");
 }
fclose(fpdata);

for (critdex=0;critdex<NCRIT2;critdex++)
 {
  for (ydex=0;ydex<ydim;ydex++)
   for (xdex=0;xdex<xdim;xdex++)
    {
     crit2n[ydex][xdex][critdex]=0;
     crit2ave[ydex][xdex][critdex]=0.0;
    }
  for (framedex=0;framedex<NFRAMES;framedex++)
   if (rtx[framedex]>0.0 && rty[framedex]>0.0)
    {
     rtxf=rtx[framedex]-floorf(rtx[framedex]);
     rtxi=(int)floorf(rtx[framedex]);
     if (rtxf>=0.5)
      {
      rtxi++;
      rtxf=1.0-rtxf;
      }
     rtyf=rty[framedex]-floorf(rty[framedex]);
     rtyi=(int)floorf(rty[framedex]);
     if (rtyf>=0.5)
      {
      rtyi++;
      rtyf=1.0-rtyf;
      }
     if (sqrt(rtxf*rtxf+rtyf*rtyf)<crit2[critdex])
      {
      crit2n[rtyi][rtxi][critdex]++;
      crit2ave[rtyi][rtxi][critdex]+=totali[rtyi][rtxi][framedex];
      }
    }
  for (ydex=0;ydex<ydim;ydex++)
   for (xdex=0;xdex<xdim;xdex++)
    if (crit2n[ydex][xdex][critdex]>0)
     crit2ave[ydex][xdex][critdex]/=crit2n[ydex][xdex][critdex];
    else
     crit2ave[ydex][xdex][critdex]=0.0;
 }
if ((fpdata=fopen("p2tmp.out","w"))==NULL)
 nrerror("Error opening traj.out");
for (ydex=0;ydex<ydim;ydex++)
 for (xdex=0;xdex<xdim;xdex++)
```

```
  {
    fprintf(fpdata,"%4d   ",ydex*xdim+xdex);
    for (critdex=0;critdex<NCRIT2;critdex++)
      fprintf(fpdata,"%8.2f %6d  ",crit2ave[ydex][xdex][critdex],crit2n[ydex][xdex][critdex]);
    fprintf(fpdata,"\n");
  }
exit(0);
```

APPENDIX F

FOCAL PLANE UNIFORMITY AND PIXEL GAP CONSIDERATIONS

It was previously determined for this sensor that an image centered on a particular pixel shares the energy from the source among four separate and surrounding pixels. A first order approximation of the total energy is often found by taking the sum of the three largest surrounding pixel values and the value recorded from the pixel the source is centered on. This is commonly referred to as the "sum of four". However, due to horizontal and vertical gaps between the pixels, some of the source energy is lost and not recorded by the detectors. Further complications arise from optical distortions and cause images to become blurred over several pixels. The total source energy can therefore spread over more than just the three adjacent pixels and all of the energy in the eight surrounding pixels must be accounted for in the summation. This type of approximation of the total energy received from a source is called a “sum of nine” [25].

Considering all of the factors mentioned above, the work of Vittitoe and George [9] attempts to quantify these errors. They use both laboratory and star source energies to establish a correction method for an image so the LD value recorded is the same as if the image were centered on a given pixel. This is estimated from actual recorded LD values for the image. The results of this work are used for sensor calibration since they better relate the actual incident energy on the FPA to the recorded LD value.

It is important to remember the pixel responses are not identical across the entire focal plane. The responses may also vary with photon wavelength. This means the pixel corrections for this focal plane vary with filter wheel position. The study does. however, conclude the pixel-to-pixel variation in filters 1, 2, and 3 is no more than a few percent.

The laboratory data used in the report yielded a pixel-to-pixel standard deviation across the entire focal plane array of 0.014. However, when the consistently noisy pixel (8,2) was removed, the standard deviation lowered to 0.006. The pixel corrections for filter wheel 4 vary considerably (up to 20%) and are reported to be a result of the detection characteristics of the HgCdTe material. Since this material is designed for high photon detectivity over a broad spectral region of tens of microns, it is difficult to accurately control the doping fraction of Cadmium in Mercury. This lack of precision causes a variation in the temperature dependent cut-off wavelength of the material and can vary substantially across the focal plane array. Since the filter wheel 4 bandwidth is near the cutoff wavelength of the detector material, there is a more significant temperature sensitivity to an individual pixel response. As a result the center of the focal plane array tends to be cooler in the center than on the outer edges, leading to a bowl shaped response

A point source at a large distance has a characteristic shape in the detection plane. Laboratory tests on this system indicated the source shape is gaussian where the 1/e position from the peak is approximately one third of a pixel side from the peak. This leads to a FWHM of about two thirds of a pixel side and is therefore slightly smaller than the size of a single pixel.

The standard deviation for gap corrections in filter wheel 4 is much larger than for filter wheels 1, 2, and 3 because: 1.) optical diffraction produces a larger image size on the focal plane at longer wavelengths and 2.) a smaller fraction of the now larger image can fall on a gap, the maximum gap correction is reduced.

APPENDIX G

STAR RADIANCE PREDICTIONS (LDS)

This appendix contains the end result prediction values, in LDs, for each star in each of the four primary sensor bands. Although the same value is used for all pixels within the field of view of the telescope, they are provided in this form to allow a one-to-one correlation between the predicted and measured pixel values for each case. Note that fractional LD values are possible since the removal of the background signal is an averaging process.

These values were calculated using 500 row, 4 column spreadsheets and are available in soft copy (Microsoft Excel format) upon request. In general the spreadsheet calculates the Engelke radiance values based on the published filter response functions for each band, sums the values for each band, and converts the value from $W/cm^2/mm$ to LDs using Equation 7 in this report.

A separate spreadsheet is used for each star in each band, identified by the title at the top of each sheet. Although there are no collected data for Alpha Centauri and Gamma Crucis in band 4, they are included for future calibrations.

2 Centauri in Band 1 (Predicted)

	0	1	2	3	4	5	6	7	8	9	10	11	12	13	14	15
15	0	0	0	0	0	0	188.0	188.0	188.0	188.0	0	0	0	0	0	0
14	0	0	0	0	0	188.0	188.0	188.0	188.0	188.0	188.0	0	0	0	0	0
13	0	0	0	0	188.0	188.0	188.0	188.0	188.0	188.0	188.0	188.0	0	0	0	0
12	0	0	0	188.0	188.0	188.0	188.0	188.0	188.0	188.0	188.0	188.0	188.0	0	0	0
11	0	0	188.0	188.0	188.0	188.0	188.0	188.0	188.0	188.0	188.0	188.0	188.0	188.0	0	0
10	0	188.0	188.0	188.0	188.0	188.0	188.0	188.0	188.0	188.0	188.0	188.0	188.0	188.0	188.0	0
9	0	188.0	188.0	188.0	188.0	188.0	188.0	188.0	188.0	188.0	188.0	188.0	188.0	188.0	188.0	0
8	188.0	188.0	188.0	188.0	188.0	188.0	188.0	188.0	188.0	188.0	188.0	188.0	188.0	188.0	188.0	188.0
7	188.0	188.0	188.0	188.0	188.0	188.0	188.0	188.0	188.0	188.0	188.0	188.0	188.0	188.0	188.0	188.0
6	0	188.0	188.0	188.0	188.0	188.0	188.0	188.0	188.0	188.0	188.0	188.0	188.0	188.0	188.0	0
5	0	188.0	188.0	188.0	188.0	188.0	188.0	188.0	188.0	188.0	188.0	188.0	188.0	188.0	188.0	0
4	0	0	188.0	188.0	188.0	188.0	188.0	188.0	188.0	188.0	188.0	188.0	188.0	188.0	0	0
3	0	0	0	188.0	188.0	188.0	188.0	188.0	188.0	188.0	188.0	188.0	188.0	0	0	0
2	0	0	0	0	188.0	188.0	188.0	188.0	188.0	188.0	188.0	188.0	0	0	0	0
1	0	0	0	0	0	188.0	188.0	188.0	188.0	188.0	188.0	0	0	0	0	0
0	0	0	0	0	0	0	188.0	188.0	188.0	188.0	0	0	0	0	0	0

2 Centauri in Band 2 (Predicted)

	0	1	2	3	4	5	6	7	8	9	10	11	12	13	14	15
15	0	0	0	0	0	0	136.5	136.5	136.5	136.5	0	0	0	0	0	0
14	0	0	0	0	0	136.5	136.5	136.5	136.5	136.5	136.5	0	0	0	0	0
13	0	0	0	0	136.5	136.5	136.5	136.5	136.5	136.5	136.5	136.5	0	0	0	0
12	0	0	0	136.5	136.5	136.5	136.5	136.5	136.5	136.5	136.5	136.5	136.5	0	0	0
11	0	0	136.5	136.5	136.5	136.5	136.5	136.5	136.5	136.5	136.5	136.5	136.5	136.5	0	0
10	0	136.5	136.5	136.5	136.5	136.5	136.5	136.5	136.5	136.5	136.5	136.5	136.5	136.5	136.5	0
9	0	136.5	136.5	136.5	136.5	136.5	136.5	136.5	136.5	136.5	136.5	136.5	136.5	136.5	136.5	0
8	136.5	136.5	136.5	136.5	136.5	136.5	136.5	136.5	136.5	136.5	136.5	136.5	136.5	136.5	136.5	136.5
7	136.5	136.5	136.5	136.5	136.5	136.5	136.5	136.5	136.5	136.5	136.5	136.5	136.5	136.5	136.5	136.5
6	0	136.5	136.5	136.5	136.5	136.5	136.5	136.5	136.5	136.5	136.5	136.5	136.5	136.5	136.5	0
5	0	136.5	136.5	136.5	136.5	136.5	136.5	136.5	136.5	136.5	136.5	136.5	136.5	136.5	136.5	0
4	0	0	136.5	136.5	136.5	136.5	136.5	136.5	136.5	136.5	136.5	136.5	136.5	136.5	0	0
3	0	0	0	136.5	136.5	136.5	136.5	136.5	136.5	136.5	136.5	136.5	136.5	0	0	0
2	0	0	0	0	136.5	136.5	136.5	136.5	136.5	136.5	136.5	136.5	0	0	0	0
1	0	0	0	0	0	136.5	136.5	136.5	136.5	136.5	136.5	0	0	0	0	0
0	0	0	0	0	0	0	136.5	136.5	136.5	136.5	0	0	0	0	0	0

2 Centauri in Band 3 (Predicted)

	0	1	2	3	4	5	6	7	8	9	10	11	12	13	14	15
15	0	0	0	0	0	0	162.9	162.9	162.9	162.9	0	0	0	0	0	0
14	0	0	0	0	0	162.9	162.9	162.9	162.9	162.9	162.9	0	0	0	0	0
13	0	0	0	0	162.9	162.9	162.9	162.9	162.9	162.9	162.9	162.9	0	0	0	0
12	0	0	0	162.9	162.9	162.9	162.9	162.9	162.9	162.9	162.9	162.9	162.9	0	0	0
11	0	0	162.9	162.9	162.9	162.9	162.9	162.9	162.9	162.9	162.9	162.9	162.9	162.9	0	0
10	0	162.9	162.9	162.9	162.9	162.9	162.9	162.9	162.9	162.9	162.9	162.9	162.9	162.9	162.9	0
9	0	162.9	162.9	162.9	162.9	162.9	162.9	162.9	162.9	162.9	162.9	162.9	162.9	162.9	162.9	0
8	162.9	162.9	162.9	162.9	162.9	162.9	162.9	162.9	162.9	162.9	162.9	162.9	162.9	162.9	162.9	162.9
7	162.9	162.9	162.9	162.9	162.9	162.9	162.9	162.9	162.9	162.9	162.9	162.9	162.9	162.9	162.9	162.9
6	0	162.9	162.9	162.9	162.9	162.9	162.9	162.9	162.9	162.9	162.9	162.9	162.9	162.9	162.9	0
5	0	162.9	162.9	162.9	162.9	162.9	162.9	162.9	162.9	162.9	162.9	162.9	162.9	162.9	162.9	0
4	0	0	162.9	162.9	162.9	162.9	162.9	162.9	162.9	162.9	162.9	162.9	162.9	162.9	0	0
3	0	0	0	162.9	162.9	162.9	162.9	162.9	162.9	162.9	162.9	162.9	162.9	0	0	0
2	0	0	0	0	162.9	162.9	162.9	162.9	162.9	162.9	162.9	162.9	0	0	0	0
1	0	0	0	0	0	162.9	162.9	162.9	162.9	162.9	162.9	0	0	0	0	0
0	0	0	0	0	0	0	162.9	162.9	162.9	162.9	0	0	0	0	0	0

2 Centauri in Band 4 (Predicted)

	0	1	2	3	4	5	6	7	8	9	10	11	12	13	14	15
15	0	0	0	0	0	0	53.6	53.6	53.6	53.6	0	0	0	0	0	0
14	0	0	0	0	0	53.6	53.6	53.6	53.6	53.6	53.6	0	0	0	0	0
13	0	0	0	0	53.6	53.6	53.6	53.6	53.6	53.6	53.6	53.6	0	0	0	0
12	0	0	0	53.6	53.6	53.6	53.6	53.6	53.6	53.6	53.6	53.6	53.6	0	0	0
11	0	0	53.6	53.6	53.6	53.6	53.6	53.6	53.6	53.6	53.6	53.6	53.6	53.6	0	0
10	0	53.6	53.6	53.6	53.6	53.6	53.6	53.6	53.6	53.6	53.6	53.6	53.6	53.6	53.6	0
9	0	53.6	53.6	53.6	53.6	53.6	53.6	53.6	53.6	53.6	53.6	53.6	53.6	53.6	53.6	0
8	53.6	53.6	53.6	53.6	53.6	53.6	53.6	53.6	53.6	53.6	53.6	53.6	53.6	53.6	53.6	53.6
7	53.6	53.6	53.6	53.6	53.6	53.6	53.6	53.6	53.6	53.6	53.6	53.6	53.6	53.6	53.6	53.6
6	0	53.6	53.6	53.6	53.6	53.6	53.6	53.6	53.6	53.6	53.6	53.6	53.6	53.6	53.6	0
5	0	53.6	53.6	53.6	53.6	53.6	53.6	53.6	53.6	53.6	53.6	53.6	53.6	53.6	53.6	0
4	0	0	53.6	53.6	53.6	53.6	53.6	53.6	53.6	53.6	53.6	53.6	53.6	53.6	0	0
3	0	0	0	53.6	53.6	53.6	53.6	53.6	53.6	53.6	53.6	53.6	53.6	0	0	0
2	0	0	0	0	53.6	53.6	53.6	53.6	53.6	53.6	53.6	53.6	0	0	0	0
1	0	0	0	0	0	53.6	53.6	53.6	53.6	53.6	53.6	0	0	0	0	0
0	0	0	0	0	0	0	53.6	53.6	53.6	53.6	0	0	0	0	0	0

Alpha Centauri in Band 1 (Predicted)

15	0	0	0	0	0	0	172.3	172.3	172.3	172.3	0	0	0	0	0	0
14	0	0	0	0	0	172.3	172.3	172.3	172.3	172.3	172.3	0	0	0	0	0
13	0	0	0	0	172.3	172.3	172.3	172.3	172.3	172.3	172.3	172.3	0	0	0	0
12	0	0	0	172.3	172.3	172.3	172.3	172.3	172.3	172.3	172.3	172.3	172.3	0	0	0
11	0	0	172.3	172.3	172.3	172.3	172.3	172.3	172.3	172.3	172.3	172.3	172.3	172.3	0	0
10	0	172.3	172.3	172.3	172.3	172.3	172.3	172.3	172.3	172.3	172.3	172.3	172.3	172.3	172.3	0
9	0	172.3	172.3	172.3	172.3	172.3	172.3	172.3	172.3	172.3	172.3	172.3	172.3	172.3	172.3	0
8	172.3	172.3	172.3	172.3	172.3	172.3	172.3	172.3	172.3	172.3	172.3	172.3	172.3	172.3	172.3	172.3
7	172.3	172.3	172.3	172.3	172.3	172.3	172.3	172.3	172.3	172.3	172.3	172.3	172.3	172.3	172.3	172.3
6	0	172.3	172.3	172.3	172.3	172.3	172.3	172.3	172.3	172.3	172.3	172.3	172.3	172.3	172.3	0
5	0	172.3	172.3	172.3	172.3	172.3	172.3	172.3	172.3	172.3	172.3	172.3	172.3	172.3	172.3	0
4	0	0	172.3	172.3	172.3	172.3	172.3	172.3	172.3	172.3	172.3	172.3	172.3	172.3	0	0
3	0	0	0	172.3	172.3	172.3	172.3	172.3	172.3	172.3	172.3	172.3	172.3	0	0	0
2	0	0	0	0	172.3	172.3	172.3	172.3	172.3	172.3	172.3	172.3	0	0	0	0
1	0	0	0	0	0	172.3	172.3	172.3	172.3	172.3	172.3	0	0	0	0	0
0	0	0	0	0	0	0	172.3	172.3	172.3	172.3	0	0	0	0	0	0

Alpha Centauri in Band 2 (Predicted)

	0	1	2	3	4	5	6	7	8	9	10	11	12	13	14	15
15	0	0	0	0	0	0	119.7	119.7	119.7	119.7	0	0	0	0	0	0
14	0	0	0	0	0	119.7	119.7	119.7	119.7	119.7	119.7	0	0	0	0	0
13	0	0	0	0	119.7	119.7	119.7	119.7	119.7	119.7	119.7	119.7	0	0	0	0
12	0	0	0	119.7	119.7	119.7	119.7	119.7	119.7	119.7	119.7	119.7	119.7	0	0	0
11	0	0	119.7	119.7	119.7	119.7	119.7	119.7	119.7	119.7	119.7	119.7	119.7	119.7	0	0
10	0	119.7	119.7	119.7	119.7	119.7	119.7	119.7	119.7	119.7	119.7	119.7	119.7	119.7	119.7	0
9	0	119.7	119.7	119.7	119.7	119.7	119.7	119.7	119.7	119.7	119.7	119.7	119.7	119.7	119.7	0
8	119.7	119.7	119.7	119.7	119.7	119.7	119.7	119.7	119.7	119.7	119.7	119.7	119.7	119.7	119.7	119.7
7	119.7	119.7	119.7	119.7	119.7	119.7	119.7	119.7	119.7	119.7	119.7	119.7	119.7	119.7	119.7	119.7
6	0	119.7	119.7	119.7	119.7	119.7	119.7	119.7	119.7	119.7	119.7	119.7	119.7	119.7	119.7	0
5	0	119.7	119.7	119.7	119.7	119.7	119.7	119.7	119.7	119.7	119.7	119.7	119.7	119.7	119.7	0
4	0	0	119.7	119.7	119.7	119.7	119.7	119.7	119.7	119.7	119.7	119.7	119.7	119.7	0	0
3	0	0	0	119.7	119.7	119.7	119.7	119.7	119.7	119.7	119.7	119.7	119.7	0	0	0
2	0	0	0	0	119.7	119.7	119.7	119.7	119.7	119.7	119.7	119.7	0	0	0	0
1	0	0	0	0	0	119.7	119.7	119.7	119.7	119.7	119.7	0	0	0	0	0
0	0	0	0	0	0	0	119.7	119.7	119.7	119.7	0	0	0	0	0	0

Alpha Centauri in Band 3 (Predicted)

	0	1	2	3	4	5	6	7	8	9	10	11	12	13	14	15
15	0	0	0	0	0	0	137.1	137.1	137.1	137.1	0	0	0	0	0	0
14	0	0	0	0	0	137.1	137.1	137.1	137.1	137.1	137.1	0	0	0	0	0
13	0	0	0	0	137.1	137.1	137.1	137.1	137.1	137.1	137.1	137.1	0	0	0	0
12	0	0	0	137.1	137.1	137.1	137.1	137.1	137.1	137.1	137.1	137.1	137.1	0	0	0
11	0	0	137.1	137.1	137.1	137.1	137.1	137.1	137.1	137.1	137.1	137.1	137.1	137.1	0	0
10	0	137.1	137.1	137.1	137.1	137.1	137.1	137.1	137.1	137.1	137.1	137.1	137.1	137.1	137.1	0
9	0	137.1	137.1	137.1	137.1	137.1	137.1	137.1	137.1	137.1	137.1	137.1	137.1	137.1	137.1	0
8	137.1	137.1	137.1	137.1	137.1	137.1	137.1	137.1	137.1	137.1	137.1	137.1	137.1	137.1	137.1	137.1
7	137.1	137.1	137.1	137.1	137.1	137.1	137.1	137.1	137.1	137.1	137.1	137.1	137.1	137.1	137.1	137.1
6	0	137.1	137.1	137.1	137.1	137.1	137.1	137.1	137.1	137.1	137.1	137.1	137.1	137.1	137.1	0
5	0	137.1	137.1	137.1	137.1	137.1	137.1	137.1	137.1	137.1	137.1	137.1	137.1	137.1	137.1	0
4	0	0	137.1	137.1	137.1	137.1	137.1	137.1	137.1	137.1	137.1	137.1	137.1	137.1	0	0
3	0	0	0	137.1	137.1	137.1	137.1	137.1	137.1	137.1	137.1	137.1	137.1	0	0	0
2	0	0	0	0	137.1	137.1	137.1	137.1	137.1	137.1	137.1	137.1	0	0	0	0
1	0	0	0	0	0	137.1	137.1	137.1	137.1	137.1	137.1	0	0	0	0	0
0	0	0	0	0	0	0	137.1	137.1	137.1	137.1	0	0	0	0	0	0

Alpha Centauri in Band 4 (Predicted)

	0	1	2	3	4	5	6	7	8	9	10	11	12	13	14	15
15	0	0	0	0	0	0	43.4	43.4	43.4	43.4	0	0	0	0	0	0
14	0	0	0	0	0	43.4	43.4	43.4	43.4	43.4	43.4	0	0	0	0	0
13	0	0	0	0	43.4	43.4	43.4	43.4	43.4	43.4	43.4	43.4	0	0	0	0
12	0	0	0	43.4	43.4	43.4	43.4	43.4	43.4	43.4	43.4	43.4	43.4	0	0	0
11	0	0	43.4	43.4	43.4	43.4	43.4	43.4	43.4	43.4	43.4	43.4	43.4	43.4	0	0
10	0	43.4	43.4	43.4	43.4	43.4	43.4	43.4	43.4	43.4	43.4	43.4	43.4	43.4	43.4	0
9	0	43.4	43.4	43.4	43.4	43.4	43.4	43.4	43.4	43.4	43.4	43.4	43.4	43.4	43.4	0
8	43.4	43.4	43.4	43.4	43.4	43.4	43.4	43.4	43.4	43.4	43.4	43.4	43.4	43.4	43.4	43.4
7	43.4	43.4	43.4	43.4	43.4	43.4	43.4	43.4	43.4	43.4	43.4	43.4	43.4	43.4	43.4	43.4
6	0	43.4	43.4	43.4	43.4	43.4	43.4	43.4	43.4	43.4	43.4	43.4	43.4	43.4	43.4	0
5	0	43.4	43.4	43.4	43.4	43.4	43.4	43.4	43.4	43.4	43.4	43.4	43.4	43.4	43.4	0
4	0	0	43.4	43.4	43.4	43.4	43.4	43.4	43.4	43.4	43.4	43.4	43.4	43.4	0	0
3	0	0	0	43.4	43.4	43.4	43.4	43.4	43.4	43.4	43.4	43.4	43.4	0	0	0
2	0	0	0	0	43.4	43.4	43.4	43.4	43.4	43.4	43.4	43.4	0	0	0	0
1	0	0	0	0	0	43.4	43.4	43.4	43.4	43.4	43.4	0	0	0	0	0
0	0	0	0	0	0	0	43.4	43.4	43.4	43.4	0	0	0	0	0	0

Gamma Crucis in Band 1 (Predicted)

	0	1	2	3	4	5	6	7	8	9	10	11	12	13	14	15
15	0	0	0	0	0	0	702.0	702.0	702.0	702.0	0	0	0	0	0	0
14	0	0	0	0	0	702.0	702.0	702.0	702.0	702.0	702.0	0	0	0	0	0
13	0	0	0	0	702.0	702.0	702.0	702.0	702.0	702.0	702.0	702.0	0	0	0	0
12	0	0	0	702.0	702.0	702.0	702.0	702.0	702.0	702.0	702.0	702.0	702.0	0	0	0
11	0	0	702.0	702.0	702.0	702.0	702.0	702.0	702.0	702.0	702.0	702.0	702.0	702.0	0	0
10	0	702.0	702.0	702.0	702.0	702.0	702.0	702.0	702.0	702.0	702.0	702.0	702.0	702.0	702.0	0
9	0	702.0	702.0	702.0	702.0	702.0	702.0	702.0	702.0	702.0	702.0	702.0	702.0	702.0	702.0	0
8	702.0	702.0	702.0	702.0	702.0	702.0	702.0	702.0	702.0	702.0	702.0	702.0	702.0	702.0	702.0	702.0
7	702.0	702.0	702.0	702.0	702.0	702.0	702.0	702.0	702.0	702.0	702.0	702.0	702.0	702.0	702.0	702.0
6	0	702.0	702.0	702.0	702.0	702.0	702.0	702.0	702.0	702.0	702.0	702.0	702.0	702.0	702.0	0
5	0	702.0	702.0	702.0	702.0	702.0	702.0	702.0	702.0	702.0	702.0	702.0	702.0	702.0	702.0	0
4	0	0	702.0	702.0	702.0	702.0	702.0	702.0	702.0	702.0	702.0	702.0	702.0	702.0	0	0
3	0	0	0	702.0	702.0	702.0	702.0	702.0	702.0	702.0	702.0	702.0	702.0	0	0	0
2	0	0	0	0	702.0	702.0	702.0	702.0	702.0	702.0	702.0	702.0	0	0	0	0
1	0	0	0	0	0	702.0	702.0	702.0	702.0	702.0	702.0	0	0	0	0	0
0	0	0	0	0	0	0	702.0	702.0	702.0	702.0	0	0	0	0	0	0

Gamma Crucis in Band 2 (Predicted)

	0	1	2	3	4	5	6	7	8	9	10	11	12	13	14	15
15	0	0	0	0	0	0	508.0	508.0	508.0	508.0	0	0	0	0	0	0
14	0	0	0	0	0	508.0	508.0	508.0	508.0	508.0	508.0	0	0	0	0	0
13	0	0	0	0	508.0	508.0	508.0	508.0	508.0	508.0	508.0	508.0	0	0	0	0
12	0	0	0	508.0	508.0	508.0	508.0	508.0	508.0	508.0	508.0	508.0	508.0	0	0	0
11	0	0	508.0	508.0	508.0	508.0	508.0	508.0	508.0	508.0	508.0	508.0	508.0	508.0	0	0
10	0	508.0	508.0	508.0	508.0	508.0	508.0	508.0	508.0	508.0	508.0	508.0	508.0	508.0	508.0	0
9	0	508.0	508.0	508.0	508.0	508.0	508.0	508.0	508.0	508.0	508.0	508.0	508.0	508.0	508.0	0
8	508.0	508.0	508.0	508.0	508.0	508.0	508.0	508.0	508.0	508.0	508.0	508.0	508.0	508.0	508.0	508.0
7	508.0	508.0	508.0	508.0	508.0	508.0	508.0	508.0	508.0	508.0	508.0	508.0	508.0	508.0	508.0	508.0
6	0	508.0	508.0	508.0	508.0	508.0	508.0	508.0	508.0	508.0	508.0	508.0	508.0	508.0	508.0	0
5	0	508.0	508.0	508.0	508.0	508.0	508.0	508.0	508.0	508.0	508.0	508.0	508.0	508.0	508.0	0
4	0	0	508.0	508.0	508.0	508.0	508.0	508.0	508.0	508.0	508.0	508.0	508.0	508.0	0	0
3	0	0	0	508.0	508.0	508.0	508.0	508.0	508.0	508.0	508.0	508.0	508.0	0	0	0
2	0	0	0	0	508.0	508.0	508.0	508.0	508.0	508.0	508.0	508.0	0	0	0	0
1	0	0	0	0	0	508.0	508.0	508.0	508.0	508.0	508.0	0	0	0	0	0
0	0	0	0	0	0	0	508.0	508.0	508.0	508.0	0	0	0	0	0	0

Gamma Crucis in Band 3 (Predicted)

	0	1	2	3	4	5	6	7	8	9	10	11	12	13	14	15
15	0	0	0	0	0	0	605.0	605.0	605.0	605.0	0	0	0	0	0	0
14	0	0	0	0	0	605.0	605.0	605.0	605.0	605.0	605.0	0	0	0	0	0
13	0	0	0	0	605.0	605.0	605.0	605.0	605.0	605.0	605.0	605.0	0	0	0	0
12	0	0	0	605.0	605.0	605.0	605.0	605.0	605.0	605.0	605.0	605.0	605.0	0	0	0
11	0	0	605.0	605.0	605.0	605.0	605.0	605.0	605.0	605.0	605.0	605.0	605.0	605.0	0	0
10	0	605.0	605.0	605.0	605.0	605.0	605.0	605.0	605.0	605.0	605.0	605.0	605.0	605.0	605.0	0
9	0	605.0	605.0	605.0	605.0	605.0	605.0	605.0	605.0	605.0	605.0	605.0	605.0	605.0	605.0	0
8	605.0	605.0	605.0	605.0	605.0	605.0	605.0	605.0	605.0	605.0	605.0	605.0	605.0	605.0	605.0	605.0
7	605.0	605.0	605.0	605.0	605.0	605.0	605.0	605.0	605.0	605.0	605.0	605.0	605.0	605.0	605.0	605.0
6	0	605.0	605.0	605.0	605.0	605.0	605.0	605.0	605.0	605.0	605.0	605.0	605.0	605.0	605.0	0
5	0	605.0	605.0	605.0	605.0	605.0	605.0	605.0	605.0	605.0	605.0	605.0	605.0	605.0	605.0	0
4	0	0	605.0	605.0	605.0	605.0	605.0	605.0	605.0	605.0	605.0	605.0	605.0	605.0	0	0
3	0	0	0	605.0	605.0	605.0	605.0	605.0	605.0	605.0	605.0	605.0	605.0	0	0	0
2	0	0	0	0	605.0	605.0	605.0	605.0	605.0	605.0	605.0	605.0	0	0	0	0
1	0	0	0	0	0	605.0	605.0	605.0	605.0	605.0	605.0	0	0	0	0	0
0	0	0	0	0	0	0	605.0	605.0	605.0	605.0	0	0	0	0	0	0

Gamma Crucis in Band 4 (Predicted)

	0	1	2	3	4	5	6	7	8	9	10	11	12	13	14	15
15	0	0	0	0	0	0	198.0	198.0	198.0	198.0	0	0	0	0	0	0
14	0	0	0	0	0	198.0	198.0	198.0	198.0	198.0	198.0	0	0	0	0	0
13	0	0	0	0	198.0	198.0	198.0	198.0	198.0	198.0	198.0	198.0	0	0	0	0
12	0	0	0	198.0	198.0	198.0	198.0	198.0	198.0	198.0	198.0	198.0	198.0	0	0	0
11	0	0	198.0	198.0	198.0	198.0	198.0	198.0	198.0	198.0	198.0	198.0	198.0	198.0	0	0
10	0	198.0	198.0	198.0	198.0	198.0	198.0	198.0	198.0	198.0	198.0	198.0	198.0	198.0	198.0	0
9	0	198.0	198.0	198.0	198.0	198.0	198.0	198.0	198.0	198.0	198.0	198.0	198.0	198.0	198.0	0
8	198.0	198.0	198.0	198.0	198.0	198.0	198.0	198.0	198.0	198.0	198.0	198.0	198.0	198.0	198.0	198.0
7	198.0	198.0	198.0	198.0	198.0	198.0	198.0	198.0	198.0	198.0	198.0	198.0	198.0	198.0	198.0	198.0
6	0	198.0	198.0	198.0	198.0	198.0	198.0	198.0	198.0	198.0	198.0	198.0	198.0	198.0	198.0	0
5	0	198.0	198.0	198.0	198.0	198.0	198.0	198.0	198.0	198.0	198.0	198.0	198.0	198.0	198.0	0
4	0	0	198.0	198.0	198.0	198.0	198.0	198.0	198.0	198.0	198.0	198.0	198.0	198.0	0	0
3	0	0	0	198.0	198.0	198.0	198.0	198.0	198.0	198.0	198.0	198.0	198.0	0	0	0
2	0	0	0	0	198.0	198.0	198.0	198.0	198.0	198.0	198.0	198.0	0	0	0	0
1	0	0	0	0	0	198.0	198.0	198.0	198.0	198.0	198.0	0	0	0	0	0
0	0	0	0	0	0	0	198.0	198.0	198.0	198.0	0	0	0	0	0	0

Lambda Velorum in Band 1 (Predicted)

	0	1	2	3	4	5	6	7	8	9	10	11	12	13	14	15
15	0	0	0	0	0	0	584.0	584.0	584.0	584.0	0	0	0	0	0	0
14	0	0	0	0	0	584.0	584.0	584.0	584.0	584.0	584.0	0	0	0	0	0
13	0	0	0	0	584.0	584.0	584.0	584.0	584.0	584.0	584.0	584.0	0	0	0	0
12	0	0	0	584.0	584.0	584.0	584.0	584.0	584.0	584.0	584.0	584.0	584.0	0	0	0
11	0	0	584.0	584.0	584.0	584.0	584.0	584.0	584.0	584.0	584.0	584.0	584.0	584.0	0	0
10	0	584.0	584.0	584.0	584.0	584.0	584.0	584.0	584.0	584.0	584.0	584.0	584.0	584.0	584.0	0
9	0	584.0	584.0	584.0	584.0	584.0	584.0	584.0	584.0	584.0	584.0	584.0	584.0	584.0	584.0	0
8	584.0	584.0	584.0	584.0	584.0	584.0	584.0	584.0	584.0	584.0	584.0	584.0	584.0	584.0	584.0	584.0
7	584.0	584.0	584.0	584.0	584.0	584.0	584.0	584.0	584.0	584.0	584.0	584.0	584.0	584.0	584.0	584.0
6	0	584.0	584.0	584.0	584.0	584.0	584.0	584.0	584.0	584.0	584.0	584.0	584.0	584.0	584.0	0
5	0	584.0	584.0	584.0	584.0	584.0	584.0	584.0	584.0	584.0	584.0	584.0	584.0	584.0	584.0	0
4	0	0	584.0	584.0	584.0	584.0	584.0	584.0	584.0	584.0	584.0	584.0	584.0	584.0	0	0
3	0	0	0	584.0	584.0	584.0	584.0	584.0	584.0	584.0	584.0	584.0	584.0	0	0	0
2	0	0	0	0	584.0	584.0	584.0	584.0	584.0	584.0	584.0	584.0	0	0	0	0
1	0	0	0	0	0	584.0	584.0	584.0	584.0	584.0	584.0	0	0	0	0	0
0	0	0	0	0	0	0	584.0	584.0	584.0	584.0	0	0	0	0	0	0

Lambda Velorum in Band 2 (Predicted)

	0	1	2	3	4	5	6	7	8	9	10	11	12	13	14	15
15	0	0	0	0	0	0	418.0	418.0	418.0	418.0	0	0	0	0	0	0
14	0	0	0	0	0	418.0	418.0	418.0	418.0	418.0	418.0	0	0	0	0	0
13	0	0	0	0	418.0	418.0	418.0	418.0	418.0	418.0	418.0	418.0	0	0	0	0
12	0	0	0	418.0	418.0	418.0	418.0	418.0	418.0	418.0	418.0	418.0	418.0	0	0	0
11	0	0	418.0	418.0	418.0	418.0	418.0	418.0	418.0	418.0	418.0	418.0	418.0	418.0	0	0
10	0	418.0	418.0	418.0	418.0	418.0	418.0	418.0	418.0	418.0	418.0	418.0	418.0	418.0	418.0	0
9	0	418.0	418.0	418.0	418.0	418.0	418.0	418.0	418.0	418.0	418.0	418.0	418.0	418.0	418.0	0
8	418.0	418.0	418.0	418.0	418.0	418.0	418.0	418.0	418.0	418.0	418.0	418.0	418.0	418.0	418.0	418.0
7	418.0	418.0	418.0	418.0	418.0	418.0	418.0	418.0	418.0	418.0	418.0	418.0	418.0	418.0	418.0	418.0
6	0	418.0	418.0	418.0	418.0	418.0	418.0	418.0	418.0	418.0	418.0	418.0	418.0	418.0	418.0	0
5	0	418.0	418.0	418.0	418.0	418.0	418.0	418.0	418.0	418.0	418.0	418.0	418.0	418.0	418.0	0
4	0	0	418.0	418.0	418.0	418.0	418.0	418.0	418.0	418.0	418.0	418.0	418.0	418.0	0	0
3	0	0	0	418.0	418.0	418.0	418.0	418.0	418.0	418.0	418.0	418.0	418.0	0	0	0
2	0	0	0	0	418.0	418.0	418.0	418.0	418.0	418.0	418.0	418.0	0	0	0	0
1	0	0	0	0	0	418.0	418.0	418.0	418.0	418.0	418.0	0	0	0	0	0
0	0	0	0	0	0	0	418.0	418.0	418.0	418.0	0	0	0	0	0	0

Lambda Velorum in Band 3 (Predicted)

	0	1	2	3	4	5	6	7	8	9	10	11	12	13	14	15
15	0	0	0	0	0	0	493.0	493.0	493.0	493.0	0	0	0	0	0	0
14	0	0	0	0	0	493.0	493.0	493.0	493.0	493.0	493.0	0	0	0	0	0
13	0	0	0	0	493.0	493.0	493.0	493.0	493.0	493.0	493.0	493.0	0	0	0	0
12	0	0	0	493.0	493.0	493.0	493.0	493.0	493.0	493.0	493.0	493.0	493.0	0	0	0
11	0	0	493.0	493.0	493.0	493.0	493.0	493.0	493.0	493.0	493.0	493.0	493.0	493.0	0	0
10	0	493.0	493.0	493.0	493.0	493.0	493.0	493.0	493.0	493.0	493.0	493.0	493.0	493.0	493.0	0
9	0	493.0	493.0	493.0	493.0	493.0	493.0	493.0	493.0	493.0	493.0	493.0	493.0	493.0	493.0	0
8	493.0	493.0	493.0	493.0	493.0	493.0	493.0	493.0	493.0	493.0	493.0	493.0	493.0	493.0	493.0	493.0
7	493.0	493.0	493.0	493.0	493.0	493.0	493.0	493.0	493.0	493.0	493.0	493.0	493.0	493.0	493.0	493.0
6	0	493.0	493.0	493.0	493.0	493.0	493.0	493.0	493.0	493.0	493.0	493.0	493.0	493.0	493.0	0
5	0	493.0	493.0	493.0	493.0	493.0	493.0	493.0	493.0	493.0	493.0	493.0	493.0	493.0	493.0	0
4	0	0	493.0	493.0	493.0	493.0	493.0	493.0	493.0	493.0	493.0	493.0	493.0	493.0	0	0
3	0	0	0	493.0	493.0	493.0	493.0	493.0	493.0	493.0	493.0	493.0	493.0	0	0	0
2	0	0	0	0	493.0	493.0	493.0	493.0	493.0	493.0	493.0	493.0	0	0	0	0
1	0	0	0	0	0	493.0	493.0	493.0	493.0	493.0	493.0	0	0	0	0	0
0	0	0	0	0	0	0	493.0	493.0	493.0	493.0	0	0	0	0	0	0

Lambda Velorum in Band 4 (Predicted)

	0	1	2	3	4	5	6	7	8	9	10	11	12	13	14	15
15	0	0	0	0	0	0	160.0	160.0	160.0	160.0	0	0	0	0	0	0
14	0	0	0	0	0	160.0	160.0	160.0	160.0	160.0	160.0	0	0	0	0	0
13	0	0	0	0	160.0	160.0	160.0	160.0	160.0	160.0	160.0	160.0	0	0	0	0
12	0	0	0	160.0	160.0	160.0	160.0	160.0	160.0	160.0	160.0	160.0	160.0	0	0	0
11	0	0	160.0	160.0	160.0	160.0	160.0	160.0	160.0	160.0	160.0	160.0	160.0	160.0	0	0
10	0	160.0	160.0	160.0	160.0	160.0	160.0	160.0	160.0	160.0	160.0	160.0	160.0	160.0	160.0	0
9	0	160.0	160.0	160.0	160.0	160.0	160.0	160.0	160.0	160.0	160.0	160.0	160.0	160.0	160.0	0
8	160.0	160.0	160.0	160.0	160.0	160.0	160.0	160.0	160.0	160.0	160.0	160.0	160.0	160.0	160.0	160.0
7	160.0	160.0	160.0	160.0	160.0	160.0	160.0	160.0	160.0	160.0	160.0	160.0	160.0	160.0	160.0	160.0
6	0	160.0	160.0	160.0	160.0	160.0	160.0	160.0	160.0	160.0	160.0	160.0	160.0	160.0	160.0	0
5	0	160.0	160.0	160.0	160.0	160.0	160.0	160.0	160.0	160.0	160.0	160.0	160.0	160.0	160.0	0
4	0	0	160.0	160.0	160.0	160.0	160.0	160.0	160.0	160.0	160.0	160.0	160.0	160.0	0	0
3	0	0	0	160.0	160.0	160.0	160.0	160.0	160.0	160.0	160.0	160.0	160.0	0	0	0
2	0	0	0	0	160.0	160.0	160.0	160.0	160.0	160.0	160.0	160.0	0	0	0	0
1	0	0	0	0	0	160.0	160.0	160.0	160.0	160.0	160.0	0	0	0	0	0
0	0	0	0	0	0	0	160.0	160.0	160.0	160.0	0	0	0	0	0	0

APPENDIX H

STAR MEASUREMENTS (LDs)

This appendix contains the consolidated pixel measurements, in LDs, for each star in each of the four primary sensor bands. Although the same value is used for all pixels within the field of view of the telescope. They are provided in this form to allow a one-to-one correlation between the predicted and measured pixel values for each case. Note that fractional LD values are possible since the removal of the background signal is an averaging process.

These values were obtained using the processing algorithm described in Chapter 3. The matrices were then consolidated on a pixel by pixel basis and recorded on a 15 x 15 focal plane map. Although only the final values are included in this report, a softcopy of the processed data tables are available on a CD ROM.

A separate spreadsheet is used for each star in each band, identified by the title at the top of each sheet. Due to collection constraints, no measurements were recorded for Alpha Centauri and Gamma Crucis in band 4. Zero values are also given for active pixels where the star never crossed the center of the pixel and therefore no meaningful data, for calibration, was obtained.

The lower half of the spreadsheet contains a 16 x 16 matrix that provides the "level-of-confidence" of each measured pixel value. Specifically, this is the number of frames the star was determined to be in the center of the pixel using the criteria outlined in Chapter 3 of this report.

2 Centauri in Band 1 (Measured)

	0	1	2	3	4	5	6	7	8	9	10	11	12	13	14	15
15	0	0	0	0	0	0	0	0	0	0	0	0	0	0	0	0
14	0	0	0	0	0	83.42	0	0	0	0	0	0	0	0	0	0
13	0	0	0	0	150.56	0	22.82	0	96.96	0	30.97	15.90	0	0	0	0
12	0	0	0	170.96	28.26	21.09	0	0	0	41.21	0	0	0	0	0	0
11	0	0	0	156.69	183.52	0	162.19	0	0	0	0	53.93	56.59	18.97	0	0
10	0	0	186.97	157.45	184.30	166.14	169.23	177.75	168.03	162.72	182.90	154.83	148.78	154.27	102.79	0
9	0	17.70	149.21	175.07	181.48	155.67	180.80	171.43	160.08	164.69	161.22	170.00	156.32	160.00	92.70	0
8	0	150.37	171.51	177.06	175.40	183.93	162.93	172.75	156.73	173.56	175.92	153.64	156.64	180.37	141.46	0
7	0	147.05	168.31	168.43	181.75	158.94	164.97	173.05	174.54	175.50	150.16	174.77	155.33	152.47	167.73	0
6	0	105.45	167.24	173.13	168.20	168.82	163.24	176.82	176.57	183.01	178.18	181.10	163.03	158.25	70.19	0
5	0	38.02	159.04	184.68	173.23	169.89	183.51	173.26	0	186.99	178.39	167.47	170.76	173.55	76.72	0
4	0	0	118.72	162.24	178.55	181.33	175.42	152.20	188.93	161.68	197.53	170.48	170.33	86.97	0	0
3	0	0	0	121.38	155.89	166.48	163.65	155.79	0	162.28	174.83	160.61	99.09	0	0	0
2	0	0	0	0	87.73	174.36	169.15	155.54	184.71	168.26	159.52	87.53	0	0	0	0
1	0	0	0	0	0	78.88	159.75	156.50	0	165.06	87.48	0	0	0	0	0
0	0	0	0	0	0	0	0	0	0	0	0	0	0	0	0	0

	0	1	2	3	4	5	6	7	8	9	10	11	12	13	14	15
15	0	0	0	0	0	0	0	0	0	0	0	0	0	0	0	0
14	0	0	0	0	0	13	0	0	0	0	0	0	0	0	0	0
13	0	0	0	0	10	0	1	0	135	0	1	1	0	0	0	0
12	0	0	0	1	1	3	0	0	0	2	0	0	0	0	0	0
11	0	0	0	6	1	0	25	0	0	0	0	2	2	1	0	0
10	0	0	10	9	3	44	28	65	18	24	32	33	4	42	109	0
9	0	3	2	4	13	20	31	15	22	9	9	8	23	19	35	0
8	0	9	29	14	16	4	24	16	4	22	3	10	13	9	2	0
7	0	11	18	12	10	20	19	21	4	14	3	4	3	20	2	0
6	0	22	17	17	9	19	20	18	3	16	3	7	11	8	45	0
5	0	1	19	19	7	15	22	18	0	15	8	14	12	16	53	0
4	0	0	29	16	13	13	16	15	4	16	13	11	1	47	0	0
3	0	0	0	39	12	17	15	14	0	12	8	3	46	0	0	0
2	0	0	0	0	40	3	15	14	1	12	6	52	0	0	0	0
1	0	0	0	0	0	22	16	6	0	8	41	0	0	0	0	0
0	0	0	0	0	0	0	0	0	0	0	0	0	0	0	0	0

2 Centauri in Band 2 (Measured)

	0	1	2	3	4	5	6	7	8	9	10	11	12	13	14	15
15	0	0	0	0	0	0	0	0	0	0	0	0	0	0	0	0
14	0	0	0	0	0	46.46	0	0	0	0	0	0	0	0	0	0
13	0	0	0	0	42.18	0	0	0	99.4	0	0	0	0	0	0	0
12	0	0	0	68.62	0	0	0	0	0	0	0	0	0	0	0	0
11	0	0	72.92	0	0	0	0	0	0	0	0	19.03	0	42.74	0	0
10	0	0	74.48	79.01	118.12	84.45	105.97	0	105.75	97.58	72.88	46.34	82.29	78.96	53.58	0
9	0	72.38	87.68	84.48	76.21	82.78	107.82	94.06	92.69	86.04	96.60	97.96	82.65	0	42.13	0
8	0	69.50	0	92.82	0	71.31	97.74	106.02	98.07	82.06	87.92	0	0	85.80	0	0
7	0	63.91	0	92.12	0	87.30	92.51	93.33	103.15	87.06	85.50	72.09	0	0	0	0
6	0	7.56	0	88.67	0	90.91	100.20	108.70	111.02	97.21	73.48	0	0	104.39	45.49	0
5	0	49.33	84.71	71.32	0	82.03	87.39	103.38	100.35	98.20	78.07	86.76	0	0	60.13	0
4	0	0	31.47	0	86.47	90.94	106.11	0	97.39	0	85.07	88.01	0	41.52	0	0
3	0	0	0	29.76	86.94	85.32	109.43	0	124.39	0	76.69	91.16	42.69	0	0	0
2	0	0	0	0	43.85	109.27	109.06	0	90.31	95.05	58.24	49.91	0	0	0	0
1	0	0	0	0	0	43.62	84.11	0	85.07	0	43.32	0	0	0	0	0
0	0	0	0	0	0	0	0	0	0	0	0	0	0	0	0	0

	0	1	2	3	4	5	6	7	8	9	10	11	12	13	14	15
15	0	0	0	0	0	0	0	0	0	0	0	0	0	0	0	0
14	0	0	0	0	0	5	0	0	0	0	0	0	0	0	0	0
13	0	0	0	0	7	0	0	0	379	0	0	0	0	0	0	0
12	0	0	0	22	0	0	0	0	0	0	0	0	0	0	0	0
11	0	0	10	0	0	1	0	0	0	0	0	1	0	2	0	0
10	0	0	15	7	1	20	4	0	22	2	18	1	4	10	39	0
9	0	18	2	7	31	14	6	27	6	4	25	5	1	1	30	0
8	0	18	0	19	0	3	17	18	21	14	19	0	0	18	0	0
7	0	16	0	18	0	15	8	22	5	11	15	1	0	0	0	0
6	0	1	0	15	0	12	15	17	9	18	4	0	0	1	15	0
5	0	2	3	5	0	16	11	4	10	11	11	14	0	0	28	0
4	0	0	9	0	2	11	6	0	7	0	12	3	0	19	0	0
3	0	0	0	27	4	6	5	0	1	0	1	9	32	0	0	0
2	0	0	0	0	57	3	5	0	3	1	2	31	0	0	0	0
1	0	0	0	0	0	27	10	0	3	0	18	0	0	0	0	0
0	0	0	0	0	0	0	0	0	0	0	0	0	0	0	0	0

2 Centauri in Band 3 (Measured)

	0	1	2	3	4	5	6	7	8	9	10	11	12	13	14	15
15	0	0	0	0	0	0	0	0	0	0	0	0	0	0	0	0
14	0	0	0	0	0	0	0	0	0	0	0	0	0	0	0	0
13	0	0	0	0	0	0	22.39	0	157.57	0	0	0	0	0	0	0
12	0	0	0	0	114.15	0	0	0	0	0	0	0	0	0	0	0
11	0	0	0	140.81	0	0	178.02	174.05	187.93	161.08	0	0	157.85	65.78	0	0
10	0	23.18	0	164.44	184.21	0	194.37	182.79	151.36	169.13	146.85	144.28	0	132.08	53.13	0
9	0	0	138.31	151.55	162.58	0	169.55	188.46	0	182.69	132.38	142.42	155.92	0	81.98	0
8	0	0	127.29	161.34	176.20	179.61	0	189.13	162.12	152.07	145.63	147.74	0	144.32	0	0
7	0	0	141.88	154.57	183.62	188.51	202.82	0	163.45	148.67	152.17	148.58	171.31	147.41	0	0
6	0	0	133.42	0	178.91	0	195.68	164.57	0	154.26	136.18	148.35	0	147.59	98.19	0
5	0	0	135.02	144.00	168.74	0	178.85	0	161.07	148.70	142.63	146.98	0	0	29.58	0
4	0	0	92.78	0	167.64	211.12	187.65	0	0	152.83	150.08	155.66	150.64	61.88	0	0
3	0	0	0	61.36	160.22	0	187.25	21.18	0	160.58	0	0	65.99	0	0	0
2	0	0	0	0	115.73	175.20	174.63	0	0	152.84	140.33	108.43	0	0	0	0
1	0	0	0	0	0	0	0	0	0	0	0	0	0	0	0	0
0	0	0	0	0	0	0	0	0	0	0	0	0	0	0	0	0

	0	1	2	3	4	5	6	7	8	9	10	11	12	13	14	15
15	0	0	0	0	0	0	0	0	0	0	0	0	0	0	0	0
14	0	0	0	0	0	0	0	0	0	0	0	0	0	0	0	0
13	0	0	0	0	0	0	1	0	325	0	0	0	0	0	0	0
12	0	0	0	0	4	0	0	0	0	0	0	0	0	0	0	0
11	0	0	0	17	0	0	66	74	2	34	0	0	2	46	0	0
10	0	1	0	2	13	0	1	14	8	9	27	21	0	29	66	0
9	0	0	15	9	18	0	1	5	0	6	22	13	4	0	33	0
8	0	0	12	12	20	16	0	3	11	14	12	18	0	3	0	0
7	0	0	13	10	15	22	7	0	11	21	25	17	2	6	0	0
6	0	0	11	0	15	0	4	7	0	11	13	17	0	8	3	0
5	0	0	15	8	18	0	10	0	11	18	14	11	0	0	23	0
4	0	0	21	0	17	1	11	0	0	18	3	6	1	40	0	0
3	0	0	0	47	9	0	10	1	0	14	0	0	25	0	0	0
2	0	0	0	0	16	2	5	0	0	9	3	17	0	0	0	0
1	0	0	0	0	0	0	0	0	0	0	0	0	0	0	0	0
0	0	0	0	0	0	0	0	0	0	0	0	0	0	0	0	0

2 Centauri in Band 4 (Measured)

	0	1	2	3	4	5	6	7	8	9	10	11	12	13	14	15
15	0	0	0	0	0	0	0	0	0	0	0	0	0	0	0	0
14	0	0	0	0	0	30.33	0	31.94	0	0	4.09	0	0	0	0	0
13	0	0	0	0	21.39	37.88	86.89	10.66	120.19	81.91	71.30	55.65	0	0	0	0
12	0	0	0	16.15	0	114.63	84.83	70.13	53.43	62.42	89.01	83.06	43.43	0	0	0
11	0	0	0	6.33	68.93	27.48	70.17	72.38	81.84	62.89	59.09	55.43	69.22	44.62	0	0
10	0	0	0	74.47	87.63	103.16	76.74	81.50	69.31	56.48	59.29	48.02	50.75	54.36	43.38	0
9	0	24.70	0	102.71	88.36	75.33	84.21	76.58	54.95	76.37	56.62	61.98	47.41	45.44	27.17	0
8	0	11.51	0	70.09	87.19	93.13	81.62	73.87	69.93	49.56	62.49	61.71	73.52	57.99	56.32	0
7	0	0	0	90.83	83.94	107.25	96.03	75.51	50.46	57.61	74.52	55.50	69.52	52.95	48.68	0
6	0	25.43	0	66.91	79.13	100.31	81.79	59.58	59.22	62.82	82.21	60.85	76.02	63.64	62.33	0
5	0	23.96	0	62.29	80.07	79.41	69.24	69.04	63.49	65.18	64.20	76.68	83.36	82.37	34.98	0
4	0	0	52.93	46.36	69.65	83.57	73.65	64.53	59.93	55.03	48.00	61.36	78.29	41.03	0	0
3	0	0	0	45.81	46.48	70.85	65.75	52.05	53.59	43.36	54.45	71.77	41.59	0	0	0
2	0	0	0	0	38.80	55.20	67.87	71.37	49.31	70.79	65.36	38.84	0	0	0	0
1	0	0	0	0	0	36.89	51.91	48.93	56.24	32.43	39.82	0	0	0	0	0
0	0	0	0	0	0	0	0	0	0	0	0	0	0	0	0	0

	0	1	2	3	4	5	6	7	8	9	10	11	12	13	14	15
15	0	0	0	0	0	0	0	0	0	0	0	0	0	0	0	0
14	0	0	0	0	0	2	0	1	0	0	4	0	0	0	0	0
13	0	0	0	0	1	1	5	1	205	8	2	11	0	0	0	0
12	0	0	0	4	0	3	48	7	4	2	1	2	20	0	0	0
11	0	0	0	1	4	1	40	22	4	1	4	6	1	11	0	0
10	0	0	0	31	51	39	41	17	33	39	40	2	22	12	78	0
9	0	7	0	22	25	4	29	26	15	5	27	25	33	22	37	0
8	0	1	0	22	4	33	44	20	7	34	33	18	19	2	15	0
7	0	0	0	15	22	23	15	26	20	17	16	4	12	18	12	0
6	0	1	0	11	19	13	24	17	20	19	13	14	11	11	29	0
5	0	1	0	6	7	17	54	17	15	13	10	1	14	14	17	0
4	0	0	2	9	4	14	36	17	15	2	3	3	8	36	0	0
3	0	0	0	20	6	3	14	15	14	5	6	10	33	0	0	0
2	0	0	0	0	13	6	14	17	11	4	9	37	0	0	0	0
1	0	0	0	0	0	10	34	9	12	1	24	0	0	0	0	0
0	0	0	0	0	0	0	0	0	0	0	0	0	0	0	0	0

Alpha Centauri in Band 1 (Measured)

	0	1	2	3	4	5	6	7	8	9	10	11	12	13	14	15
15	0	0	0	0	0	0	0	0	0	0	0	0	0	0	0	0
14	0	0	0	0	0	18.26	0	0	237.49	0	0	0	0	0	0	0
13	0	0	0	0	0	0	0	212.94	104.91	0	138609	11.37	0	0	0	0
12	0	0	0	0	0	154.57	208.94	198.91	25.45	0	0	83.54	0	0	0	0
11	0	0	0	183.94	194.72	188.97	183.29	194.80	217.23	203.41	209.52	200.40	191.88	141.99	0	0
10	0	15.34	0	195.80	197.93	188.62	201.38	199.53	226.73	6666	215.99	195.03	194.04	186.50	133.64	0
9	0	18.40	141698	223.58	206.60	188.37	203.54	190.65	200.54	215.54	206.83	199.84	199.83	189.54	164.40	0
8	0	17.12	5.93	237.23	206.32	195.10	152.56	155.72	136.26	200.26	230.27	193.12	197.52	0	176.08	0
7	0	0	0	349.36	193.16	190.06	146.11	137.07	10741	197.38	205.33	203.57	195.00	199.08	189.45	0
6	0	0	0	219.36	182.84	167.39	133.51	0	141.65	198.14	188.48	199.11	210.89	187.79	51.35	0
5	0	0	0	209.04	181.98	181.96	193.12	526.13	19169	203.20	200.38	200.88	201.26	180.02	129.27	0
4	0	0	9.28	212.64	187.07	640.97	1755	195.25	216.49	10.27	0	217.87	187.42	107.82	0	0
3	0	0	0	102.91	186.25	160.02	189.63	207.13	206.21	199.08	236.60	86057	77.48	0	0	0
2	0	0	0	0	115.88	0	177.45	187.57	224.56	86099	208.46	126.67	0	0	0	0
1	0	0	0	0	0	97.20	0	204.62	196.74	180.16	112.47	0	0	0	0	0
0	0	0	0	0	0	0	0	0	0	0	0	0	0	0	0	0
	0	**1**	**2**	**3**	**4**	**5**	**6**	**7**	**8**	**9**	**10**	**11**	**12**	**13**	**14**	**15**
15	0	0	0	0	0	0	0	0	0	0	0	0	0	0	0	0
14	0	0	0	0	0	2	0	0	2	0	0	0	0	0	0	0
13	0	0	0	0	0	0	0	3	21	0	1	1	0	0	0	0
12	0	0	0	0	0	1	10	84	1	1	0	1	0	0	0	0
11	0	0	0	20	57	91	32	134	115	31	62	114	71	132	0	0
10	0	1	0	32	70	59	90	48	85	59	19	56	23	55	74	0
9	0	1	1	11	11	84	52	23	14	38	7	50	23	15	60	0
8	0	1	1	41	8	98	39	16	7	52	8	36	48	0	14	0
7	0	0	0	59	20	68	40	13	12	24	5	30	62	13	6	0
6	0	0	0	72	40	10	15	0	8	14	11	53	18	32	74	0
5	0	0	0	35	63	5	100	5	14	11	28	50	35	10	34	0
4	0	0	1	23	43	4	73	1	23	1	0	43	33	118	0	0
3	0	0	0	80	24	3	31	3	26	22	1	48	82	0	0	0
2	0	0	0	0	92	0	14	12	39	23	2	122	0	0	0	0
1	0	0	0	0	0	75	0	48	35	19	38	0	0	0	0	0
0	0	0	0	0	0	0	0	0	0	0	0	0	0	0	0	0

Alpha Centauri in Band 2 (Measured)

	0	1	2	3	4	5	6	7	8	9	10	11	12	13	14	15
15	0	0	0	0	0	0	0	0	0	0	0	0	0	0	0	0
14	0	0	0	0	0	0	0	0	0	0	0	0	0	0	0	0
13	0	0	0	0	13.18	0	35.30	0	70.07	0	0	10.81	0	0	0	0
12	0	0	0	15.73	0	83.73	0	92.67	0	2.97	0	15.44	14.43	0	0	0
11	0	0	0	118.38	137.04	148.12	153.9	154.63	160.56	153.16	139.39	142.69	149.07	116.52	0	0
10	0	13.82	96.79	0	146.91	153.21	149.91	156.48	157.39	155.47	154.07	149.46	148.21	141.92	56.25	0
9	0	17.62	0	156.17	147.18	149.08	142.39	149.13	148.77	159.16	144.53	145.31	149.27	148.44	85.94	0
8	0	0	124.10	138.34	147.66	152.73	145.32	145.94	144.22	163.17	140.09	156.16	0	149.55	146.11	0
7	0	0	0	131.40	159.36	141.63	152.12	148.46	152.34	165.34	151.15	0	0	145.67	26.08	0
6	0	16.37	0	133.39	147.31	144.34	161.10	169.09	139.06	149.06	151.18	140.54	136.56	165.53	51.87	0
5	0	0	0	130.58	130.75	142.57	147.28	148.67	149.16	165.76	140.20	215.63	148.30	145.01	46.85	0
4	0	0	16.36	136.58	132.47	140.69	149.12	145.77	151.86	145.17	148.83	146.95	143.85	85.54	0	0
3	0	0	0	70.17	137.86	144.11	147.61	152.42	139.75	143.73	149.23	147.25	120.11	0	0	0
2	0	0	0	0	86.21	147.99	135.17	151.43	129.12	144.20	144.66	120.04	0	0	0	0
1	0	0	0	0	0	111.92	132.62	145.62	140.38	136.71	75.77	0	0	0	0	0
0	0	0	0	0	0	0	0	0	0	0	0	0	0	0	0	0

	0	1	2	3	4	5	6	7	8	9	10	11	12	13	14	15
15	0	0	0	0	0	0	0	0	0	0	0	0	0	0	0	0
14	0	0	0	0	0	0	0	0	0	0	0	0	0	0	0	0
13	0	0	0	0	1	0	1	0	135	0	0	1	0	0	0	0
12	0	0	0	1	0	1	0	2	0	1	0	1	1	0	0	0
11	0	0	0	1	131	47	111	175	136	121	103	175	55	251	0	0
10	0	3	1	0	117	33	37	34	60	44	25	26	24	35	217	0
9	0	1	0	128	67	26	49	55	26	19	18	20	19	16	85	0
8	0	0	1	19	10	50	35	76	24	7	24	7	0	21	7	0
7	0	0	0	20	5	34	15	86	9	6	37	0	0	45	1	0
6	0	1	0	2	14	38	9	46	25	16	34	5	23	73	56	0
5	0	0	0	23	5	30	37	28	69	10	35	30	42	44	70	0
4	0	0	1	28	21	25	66	32	66	33	67	66	27	146	0	0
3	0	0	0	58	24	55	44	61	48	29	50	48	26	0	0	0
2	0	0	0	0	67	73	11	67	51	30	37	68	0	0	0	0
1	0	0	0	0	0	83	11	50	32	12	124	0	0	0	0	0
0	0	0	0	0	0	0	0	0	0	0	0	0	0	0	0	0

Alpha Centauri in Band 3 (Measured)

	0	1	2	3	4	5	6	7	8	9	10	11	12	13	14	15
15	0	0	0	0	0	0	0	0	0	0	0	0	0	0	0	0
14	0	0	0	0	0	0	184.62	218.86	0	0	0	0	0	0	0	0
13	0	0	0	0	204.12	225.04	0	0	101.01	0	0	0	0	0	0	0
12	0	0	0	209.53	21.76	0	0	0	0	0	0	0	0	0	0	0
11	0	0	211.64	223.15	219.83	222.04	220.04	217.30	225.83	213.95	213.87	218.55	219.51	89.61	0	0
10	0	0	218.87	219.99	219.01	203.29	208.49	219.78	213.86	215.47	208.48	0	204.60	210.04	76.74	0
9	0	0	210.56	220.16	222.56	206.34	209.23	214.62	217.07	222.98	215.07	204.35	212.85	0	91.27	0
8	0	0	216.84	212.68	216.38	213.17	213.40	210.18	223.43	213.95	209.16	208.77	206.79	7.82	148.93	0
7	0	0	216.58	212.97	220.53	224.09	215.33	203.80	229.33	222.94	214.73	200.03	219.09	0	207.31	0
6	0	0	214.74	223.39	221.74	222.60	215.15	219.70	227.25	199.94	201.40	210.12	210.15	211.18	183.51	0
5	0	13.78	221.88	208.64	225.66	214.83	213.78	218.67	225.43	215.76	213.46	207.56	216.17	221.43	171.07	0
4	0	0	164.01	212.67	229.90	221.12	224.71	216.12	220.98	226.86	221.28	219.67	190.99	127.76	0	0
3	0	0	0	174.03	224.58	213.72	233.58	218.21	218.33	220.87	187.91	207.43	88.12	0	0	0
2	0	0	0	0	153.87	215.66	212.15	216.98	220.32	211.49	194.31	176.56	0	0	0	0
1	0	0	0	0	0	146.28	210.95	214.32	209.10	199.91	156.37	0	0	0	0	0
0	0	0	0	0	0	0	0	0	0	0	0	0	0	0	0	0
	0	**1**	**2**	**3**	**4**	**5**	**6**	**7**	**8**	**9**	**10**	**11**	**12**	**13**	**14**	**15**
15	0	0	0	0	0	0	0	0	0	0	0	0	0	0	0	0
14	0	0	0	0	0	0	1	6	0	0	0	0	0	0	0	0
13	0	0	0	0	37	10	0	0	31	0	0	0	0	0	0	0
12	0	0	0	52	1	0	0	0	0	0	0	0	0	0	0	0
11	0	0	58	218	172	199	186	177	218	247	181	166	147	194	0	0
10	0	0	64	70	10	100	32	75	69	101	9	0	47	19	215	0
9	0	0	60	64	49	71	53	49	84	56	21	3	69	0	51	0
8	0	0	67	64	87	39	61	8	70	44	25	29	70	2	5	0
7	0	0	61	90	73	91	71	16	69	44	15	16	49	0	21	0
6	0	0	61	66	69	83	67	74	67	75	35	49	6	15	78	0
5	0	1	62	65	70	65	78	51	66	66	62	86	21	41	52	0
4	0	0	64	73	62	64	64	82	63	67	72	85	3	195	0	0
3	0	0	0	83	47	58	62	59	61	60	61	52	29	0	0	0
2	0	0	0	0	101	45	60	59	46	62	60	48	0	0	0	0
1	0	0	0	0	0	92	44	59	48	55	76	0	0	0	0	0
0	0	0	0	0	0	0	0	0	0	0	0	0	0	0	0	0

Gamma Crucis in Band 1 (Measured)

	0	1	2	3	4	5	6	7	8	9	10	11	12	13	14	15
15	0	0	0	0	0	0	0	0	0	0	0	0	0	0	0	0
14	0	0	0	0	0	0	0	0	0	0	0	0	0	0	0	0
13	0	0	0	0	27.23	0	0	0	84.37	0	0	0	0	0	0	0
12	0	0	0	0	0	0	0	0	0	0	0	41.79	0	0	0	0
11	0	0	0	676.8	0	698.5	655.8	698.7	678.30	642.8	693.3	662.1	694.60	637	0	0
10	0	177.7	676.5	678.20	650.9	686.9	682.4	706.4	665.7	648.9	688.2	684.6	692.1	696.5	247.4	0
9	0	414.8	700.3	687.8	647.6	702.9	706.3	691.4	714.5	698.5	657	0	714.1	690.6	657.2	0
8	0	454.8	687.5	661.8	670.8	537.1	476.80	708.3	718.5	702.2	651.3	303.70	694.7	680.40	0	0
7	0	426.1	699.9	663.00	668.3	507.20	473.3	695.5	708.9	698.9	649.5	122.8	665.3	670.1	0	0
6	0	340.5	654.50	679.5	711.2	529.60	379.9	660.6	640.8	674.7	688.1	303.6	687.3	679	0	0
5	0	361.1	638.1	689.1	708.1	653.80	705.7	664.2	641.2	654.4	667.8	661.3	690.1	653.5	384.9	0
4	0	0	369.8	656.2	687.5	686.1	723	702.8	692.5	653.20	704.6	664.2	696.9	0	0	0
3	0	0	0	446.7	667.8	641.3	682.9	685.2	690.40	662.4	685.8	694.00	355	0	0	0
2	0	0	0	0	325.7	620.2	682.3	663	693.7	695.7	649.1	462.7	0	0	0	0
1	0	0	0	0	0	163.8	667.6	646.7	686.5	658	392.5	0	0	0	0	0
0	0	0	0	0	0	0	0	0	0	0	0	0	0	0	0	0

	0	1	2	3	4	5	6	7	8	9	10	11	12	13	14	15
15	0	0	0	0	0	0	0	0	0	0	0	0	0	0	0	0
14	0	0	0	0	0	0	0	0	0	0	0	0	0	0	0	0
13	0	0	0	0	1	0	0	0	20	0	0	0	0	0	0	0
12	0	0	0	0	0	0	0	0	0	0	0	1	0	0	0	0
11	0	0	0	114	0	186	5	121	90	13	108	89	135	103	0	0
10	0	115	138	135	124	105	114	76	62	46	95	76	102	156	43	0
9	0	66	19	81	47	98	90	71	25	90	63	0	28	84	39	0
8	0	3	23	43	40	34	62	60	11	81	18	45	22	132	0	0
7	0	40	28	78	63	20	57	25	15	71	45	6	9	98	0	0
6	0	64	55	78	21	13	6	38	33	63	63	71	86	109	0	0
5	0	72	87	68	5	134	4	45	12	21	38	47	75	45	48	0
4	0	0	86	31	34	74	17	60	15	14	4	45	74	0	0	0
3	0	0	0	94	41	34	76	65	34	33	10	4	139	0	0	0
2	0	0	0	0	90	9	51	93	16	66	28	81	0	0	0	0
1	0	0	0	0	0	55	4	87	4	76	99	0	0	0	0	0
0	0	0	0	0	0	0	0	0	0	0	0	0	0	0	0	0

Gamma Crucis in Band 2 (Measured)

	0	1	2	3	4	5	6	7	8	9	10	11	12	13	14	15
15	0	0	0	0	0	0	0	0	0	0	0	0	0	0	0	0
14	0	0	0	0	0	0	4.35	0	0	0	0	0	0	0	0	0
13	0	0	0	0	29.83	0	0	0	118.14	0	0	0	0	0	0	0
12	0	0	0	0	0	0	91.03	65.48	0	0	94.64	0	0	0	0	0
11	0	0	164.04	0	0	0	0	412.94	413.67	415.84	406.41	387.23	414.73	302.01	0	0
10	0	364.20	0	0	0	28.54	0	413.72	414.62	421.69	408.56	416.38	408.51	407.46	0	0
9	0	330.51	268.70	0	0	0	0	415.69	418.43	421.48	369.40	420.99	386.57	394.30	0	0
8	0	387.63	402.01	0	0	0	0	426.71	420.00	413.28	397.07	413.95	387.82	404.26	0	0
7	0	391.00	0	0	0	0	0	417.45	425.95	418.65	426.55	414.59	386.41	368.92	0	0
6	0	387.83	0	0	0	0	409.20	415.21	403.34	408.11	406.07	405.39	394.88	377.07	0	0
5	0	387.75	0	0	0	0	409.52	412.68	406.27	410.68	413.58	408.26	393.53	401.38	0	0
4	0	0	91.94	0	95.59	0	414.15	410.92	399.77	405.80	399.79	416.94	385.60	320.63	0	0
3	0	0	0	0	0	0	0	412.93	400.76	395.12	404.87	403.97	318.64	0	0	0
2	0	0	0	0	0	8.35	0	414.84	412.64	392.59	400.38	296.94	0	0	0	0
1	0	0	0	0	0	0	50.13	396.92	397.83	394.68	244.45	0	0	0	0	0
0	0	0	0	0	0	0	0	0	0	0	0	0	0	0	0	0

	0	1	2	3	4	5	6	7	8	9	10	11	12	13	14	15
15	0	0	0	0	0	0	0	0	0	0	0	0	0	0	0	0
14	0	0	0	0	0	0	1	0	0	0	0	0	0	0	0	0
13	0	0	0	0	1	0	0	0	8	0	0	0	0	0	0	0
12	0	0	0	0	0	0	4	1	0	0	1	0	0	0	0	0
11	0	0	109	0	0	0	0	96	81	57	107	49	80	199	0	0
10	0	85	0	0	0	1	0	112	107	42	51	47	10	127	0	0
9	0	31	3	0	0	0	0	94	64	40	12	18	24	55	0	0
8	0	11	15	0	0	0	0	75	72	54	6	18	11	14	0	0
7	0	21	0	0	0	0	0	100	80	30	21	20	12	69	0	0
6	0	74	0	0	0	0	5	64	86	36	68	48	4	16	0	0
5	0	10	0	0	0	0	4	71	62	84	47	68	4	38	0	0
4	0	0	64	0	1	0	4	82	83	71	55	68	55	75	0	0
3	0	0	0	0	0	0	0	64	80	67	34	89	87	0	0	0
2	0	0	0	0	0	1	0	73	65	74	38	106	0	0	0	0
1	0	0	0	0	0	0	1	64	82	50	105	0	0	0	0	0
0	0	0	0	0	0	0	0	0	0	0	0	0	0	0	0	0

Gamma Crucis in Band 3 (Measured)

	0	1	2	3	4	5	6	7	8	9	10	11	12	13	14	15
15	0	0	0	0	0	0	0	0	0	0	0	0	0	0	0	0
14	0	0	0	0	0	0	0	0	0	0	0	0	0	0	0	0
13	0	0	0	0	0	0	0	0	80.87	0	0	0	0	0	0	0
12	0	0	0	0	0	0	0	25.33	0	0	17.15	0	0	0	0	0
11	0	0	497.77	649.34	654.90	634.87	653.96	671.75	671.98	652.93	650.35	626.83	0	190.74	0	0
10	0	399.27	648.28	672.00	669.40	662.97	648.54	673.16	679.10	691.85	676.38	680.78	662.77	670.83	430.54	0
9	0	238.57	640.04	672.34	672.14	703.18	655.62	675.90	679.98	689.11	662.73	668.84	684.73	640.12	0	0
8	0	583.87	678.49	639.66	687.74	666.56	649.97	670.27	654.97	683.09	659.13	670.94	666.38	698.94	0	0
7	0	542.42	686.45	669.26	692.70	647.50	660.59	697.22	678.24	648.52	663.61	675.82	700.81	672.82	0	0
6	0	274.69	655.64	675.74	703.44	652.58	683.95	680.91	669.30	667.81	679.32	710.99	687.75	0	614.63	0
5	0	201.41	654.27	636.72	672.73	697.31	684.78	662.19	668.48	676.16	686.55	668.65	694.76	657.74	651.77	0
4	0	0	393.8	686.69	669.42	696.14	689.97	657.40	677.06	683.14	670.01	693.69	685.92	380.62	0	0
3	0	0	0	107.80	663.72	650.05	672.55	697.81	648.80	679.76	606.31	681.23	428.08	0	0	0
2	0	0	0	0	624.16	668.84	660.28	660.45	671.96	673.28	678.65	346.47	0	0	0	0
1	0	0	0	0	0	381.04	656.50	649.41	653.41	638.48	512.11	0	0	0	0	0
0	0	0	0	0	0	0	0	0	0	0	0	0	0	0	0	0

	0	1	2	3	4	5	6	7	8	9	10	11	12	13	14	15
15	0	0	0	0	0	0	0	0	0	0	0	0	0	0	0	0
14	0	0	0	0	0	0	0	0	0	0	0	0	0	0	0	0
13	0	0	0	0	0	0	0	0	6	0	0	0	0	0	0	0
12	0	0	0	0	0	0	0	1	0	0	1	0	0	0	0	0
11	0	0	166	62	23	30	80	51	103	57	79	52	0	46	0	0
10	0	30	119	54	110	37	99	109	52	36	113	197	65	11	75	0
9	0	55	80	84	73	29	92	49	86	30	103	65	90	17	0	0
8	0	28	10	36	22	37	93	87	80	17	57	47	56	13	0	0
7	0	35	15	25	15	29	94	66	70	18	16	19	78	6	0	0
6	0	78	14	10	5	7	88	72	68	13	4	25	94	0	5	0
5	0	49	40	3	18	4	87	53	59	18	6	36	44	5	21	0
4	0	0	150	5	52	6	78	10	74	15	7	30	62	84	0	0
3	0	0	0	57	40	12	67	35	76	4	13	14	108	0	0	0
2	0	0	0	0	70	60	44	40	66	43	23	143	0	0	0	0
1	0	0	0	0	0	163	62	40	61	4	25	0	0	0	0	0
0	0	0	0	0	0	0	0	0	0	0	0	0	0	0	0	0

Lambda Velorum in Band 1 (Measured)

	0	1	2	3	4	5	6	7	8	9	10	11	12	13	14	15
15	0	0	0	0	0	0	0	0	0	0	0	0	0	0	0	0
14	0	0	0	0	0	0	0	0	0	0	0	0	0	0	0	0
13	0	0	0	0	0	0	0	0	130.69	0	0	0	0	0	0	0
12	0	0	0	0	0	0	0	54.74	0	101.03	0	0	0	0	0	0
11	0	0	0	196.01	0	118.29	129.66	182.72	191.49	147.52	129.82	132.00	160.17	77.25	0	0
10	0	0	202.68	150.67	109.80	129.56	153.48	181.04	174.56	153.55	145.34	163.83	157.34	152.89	88.36	0
9	0	0	200.29	153.37	118.84	140.94	82.94	168.21	168.16	140.64	152.41	164.48	157.08	150.36	99.12	0
8	0	22.14	205.24	129.37	120.29	128.75	169.74	167.50	164.62	151.90	150.51	165.63	152.10	150.11	138.84	0
7	0	0	188.39	132.56	124.72	133.94	185.13	167.82	185.83	140.93	144.26	163.69	157.95	147.37	149.81	0
6	0	30.88	188.93	142.88	121.08	139.45	182.95	165.30	164.25	143.10	147.78	173.39	170.05	146.79	111.82	0
5	0	17.63	173.20	124.76	125.11	144.32	192.27	161.95	161.58	145.40	153.06	161.63	164.75	149.43	83.40	0
4	0	0	170.87	133.32	126.53	150.86	201.66	152.10	170.37	149.46	154.47	173.40	156.19	130.42	0	0
3	0	0	0	92.71	128.10	147.16	204.13	157.79	158.04	141.72	147.22	165.50	92.21	0	0	0
2	0	0	0	0	118.06	146.51	194.66	164.48	193.99	138.12	152.64	139.53	0	0	0	0
1	0	0	0	0	0	111.91	197.25	216.55	145.56	138.18	120.37	0	0	0	0	0
0	0	0	0	0	0	0	0	0	0	0	0	0	0	0	0	0
	0	**1**	**2**	**3**	**4**	**5**	**6**	**7**	**8**	**9**	**10**	**11**	**12**	**13**	**14**	**15**
15	0	0	0	0	0	0	0	0	0	0	0	0	0	0	0	0
14	0	0	0	0	0	0	0	0	0	0	0	0	0	0	0	0
13	0	0	0	0	0	0	0	0	221	0	0	0	0	0	0	0
12	0	0	0	0	0	0	0	1	0	3	0	0	0	0	0	0
11	0	0	0	140	0	80	63	110	101	50	29	30	48	124	0	0
10	0	0	98	161	117	139	93	96	115	101	144	111	63	87	233	0
9	0	0	46	88	45	78	1	60	28	58	72	49	15	53	154	0
8	0	1	43	66	52	46	27	64	51	103	67	71	13	72	48	0
7	0	0	63	44	61	37	95	52	75	53	79	70	78	23	74	0
6	0	1	73	40	79	45	58	61	91	51	68	104	79	38	127	0
5	0	1	53	49	39	46	46	50	52	41	51	34	48	40	202	0
4	0	0	52	63	51	61	46	63	45	40	67	38	53	47	0	0
3	0	0	0	125	75	47	59	37	48	58	63	57	65	0	0	0
2	0	0	0	0	28	69	58	65	84	44	43	121	0	0	0	0
1	0	0	0	0	0	119	66	63	61	79	92	0	0	0	0	0
0	0	0	0	0	0	0	0	0	0	0	0	0	0	0	0	0

Lambda Velorum in Band 2 (Measured)

	0	1	2	3	4	5	6	7	8	9	10	11	12	13	14	15
15	0	0	0	0	0	0	0	0	0	0	0	0	0	0	0	0
14	0	0	0	0	0	59.36	101.84	117.52	0	139.71	0	0	0	0	0	0
13	0	0	0	0	0	0	0	0	126.07	0	0	0	0	0	0	0
12	0	0	0	0	0	0	138.00	0	0	104.01	0	0	75.25	0	0	0
11	0	0	89.99	36.03	43.55	133.08	141.57	124.20	75.92	76.40	131.84	150.60	105.47	36.06	0	0
10	0	63.97	79.08	48.93	74.36	132.33	103.54	115.33	68.98	171.02	120.66	104.82	72.21	66.36	68.04	0
9	0	59.82	47.59	59.72	101.28	133.25	104.90	90.99	147.27	108.36	161.72	97.36	72.29	165.22	74.60	0
8	0	0	12.86	71.20	117.70	130.56	78.83	74.50	86.29	132.08	102.81	124.70	77.22	128.95	109.24	0
7	0	0	30.39	74.29	124.76	127.87	82.46	81.75	112.84	156.03	0	105.45	73.17	140.07	74.43	0
6	0	0	29.20	73.77	100.46	124.32	89.62	135.32	87.89	161.56	104.00	151.26	74.92	79.68	75.63	0
5	0	0	33.60	71.47	79.02	118.94	130.44	120.59	149.35	118.54	156.00	107.34	75.94	74.12	66.50	0
4	0	0	25.42	33.67	70.03	136.06	70.25	104.26	84.32	137.26	106.05	135.69	78.58	61.78	0	0
3	0	0	0	44	43.80	143.91	102.78	64.94	65.62	91.63	154.05	89.45	61.02	0	0	0
2	0	0	0	0	29.37	106.25	206.74	75.85	67.25	122.78	105.65	41.61	0	0	0	0
1	0	0	0	0	0	107.24	88.63	66.55	74.63	96.18	125.56	0	0	0	0	0
0	0	0	0	0	0	0	0	0	0	0	0	0	0	0	0	0

	0	1	2	3	4	5	6	7	8	9	10	11	12	13	14	15
15	0	0	0	0	0	0	0	0	0	0	0	0	0	0	0	0
14	0	0	0	0	0	1	1	2	0	1	0	0	0	0	0	0
13	0	0	0	0	0	0	0	0	18	0	0	0	0	0	0	0
12	0	0	0	0	0	0	23	0	0	6	0	0	14	0	0	0
11	0	0	129	142	153	73	64	285	57	250	100	212	20	47	0	0
10	0	3	51	102	50	61	17	121	26	214	31	182	65	68	225	0
9	0	12	21	59	82	60	10	59	28	57	14	64	68	16	82	0
8	0	0	27	46	82	63	23	54	48	63	9	38	74	88	30	0
7	0	0	54	68	63	67	50	49	36	51	0	16	39	47	43	0
6	0	0	54	76	20	86	33	59	34	62	6	33	46	56	50	0
5	0	0	35	64	8	26	46	53	56	62	5	19	60	47	79	0
4	0	0	17	31	18	15	111	130	98	84	22	8	38	93	0	0
3	0	0	0	58	3	43	54	70	46	20	36	39	93	0	0	0
2	0	0	0	0	19	8	33	58	29	52	11	41	0	0	0	0
1	0	0	0	0	0	14	10	37	3	54	8	0	0	0	0	0
0	0	0	0	0	0	0	0	0	0	0	0	0	0	0	0	0

Lambda Velorum in Band 3 (Measured)

	0	1	2	3	4	5	6	7	8	9	10	11	12	13	14	15
15	0	0	0	0	0	0	0	0	0	0	0	0	0	0	0	0
14	0	0	0	0	0	0	56.11	0	0	0	0	0	0	0	0	0
13	0	0	0	0	0	0	165.81	20.93	199.67	0	0	0	0	0	0	0
12	0	0	0	0	0	156.31	111.44	258.56	0	122.52	0	49.61	0	0	0	0
11	0	0	0	149.87	70.56	115.49	135.11	238.29	0	0	30.33	242.10	187.82	115.27	0	0
10	0	0	150.03	128.21	86.68	135.35	239.83	236.73	0	0	0	223.42	184.01	161.88	69.75	0
9	0	170.98	120.74	97.80	84.98	143.46	227.66	234.33	103.64	66.89	201.74	28.89	260.35	130.64	101.59	0
8	0	160.35	135.56	120.06	83.92	135.86	161.24	236.85	45.85	0	196.23	0	265.17	155.24	152.45	0
7	0	213.41	108.70	100.80	95.94	40.98	39.93	208.15	0	0	180.52	186.61	176.23	162.30	147.96	0
6	0	196.94	120.00	95.31	77.08	154.73	148.32	205.86	0	0	165.92	184.96	194.48	148.99	121.32	0
5	0	139.29	0	93.49	58.29	35.54	126.11	189.32	181.86	0	0	179.79	196.02	152.69	82.96	0
4	0	0	127.78	114.30	122.51	135.92	136.20	186.81	0	0	0	173.97	167.10	108.06	0	0
3	0	0	0	74.14	139.42	112.44	137.04	198.64	0	60.58	192.40	131.39	142.71	0	0	0
2	0	0	0	0	86.98	105.82	132.87	0	0	0	255.24	102.96	0	0	0	0
1	0	0	0	0	0	95.70	196.54	0	0	61.02	100.72	0	0	0	0	0
0	0	0	0	0	0	0	0	0	0	0	0	0	0	0	0	0

	0	1	2	3	4	5	6	7	8	9	10	11	12	13	14	15
15	0	0	0	0	0	0	0	0	0	0	0	0	0	0	0	0
14	0	0	0	0	0	0	1	0	0	0	0	0	0	0	0	0
13	0	0	0	0	0	0	1	1	210	0	0	0	0	0	0	0
12	0	0	0	0	0	1	2	8	0	2	0	1	0	0	0	0
11	0	0	0	31	1	203	5	105	0	0	1	72	19	102	0	0
10	0	0	78	46	91	95	69	29	0	0	0	86	82	112	129	0
9	0	25	9	72	45	49	50	16	2	1	52	1	41	22	53	0
8	0	83	1	29	11	41	11	14	1	0	52	0	9	59	38	0
7	0	131	2	64	7	2	11	11	0	0	59	17	11	33	37	0
6	0	51	90	107	27	15	21	7	0	0	55	48	7	53	49	0
5	0	6	0	30	65	4	56	5	3	0	0	64	6	51	109	0
4	0	0	11	9	48	14	61	9	0	0	0	92	27	281	0	0
3	0	0	0	48	72	5	61	4	0	1	2	46	88	0	0	0
2	0	0	0	0	113	5	37	0	0	0	30	62	0	0	0	0
1	0	0	0	0	0	68	49	0	0	2	15	0	0	0	0	0
0	0	0	0	0	0	0	0	0	0	0	0	0	0	0	0	0

Lambda Velorum in Band 4 (Measured)

	0	1	2	3	4	5	6	7	8	9	10	11	12	13	14	15
15	0	0	0	0	0	0	0	0	0	0	0	0	0	0	0	0
14	0	0	0	0	0	0	0	0	0	0	34.24	0	0	0	0	0
13	0	0	0	0	0	0	0	0	179.66	0	0	0	0	0	0	0
12	0	0	0	0	0	0	141.11	0	0	0	0	0	0	0	0	0
11	0	0	113.50	131.49	0	107.93	158.86	108.71	31.11	37.08	42.00	7.39	55.45	36.30	0	0
10	0	0	75.60	44.58	0	105.28	101.21	80.11	153.84	22.17	28.63	71.34	81.22	58.26	32.42	0
9	0	0	60.42	0	0	36.69	138.35	146.47	50.95	19.60	147.27	179.80	60.11	90.46	37.66	0
8	0	0	93.40	0	5.09	17.62	0	67.32	135.70	186.24	156.72	68.55	71.58	80.80	40.95	0
7	0	0	16.98	0	0	16.25	128.13	70.51	170.73	162.71	200.60	75.68	60.89	94.76	74.19	0
6	0	95.83	25.09	0	0.88	6.98	136.75	79.21	67.93	180.60	39.58	203.26	58.08	175.85	20.26	0
5	0	49.16	32.69	4.71	5.65	67.10	133.10	132.41	222.26	189.84	53.72	167.24	65.81	47.49	32.28	0
4	0	0	28.79	8.48	13.82	61.53	112.74	117.09	26.58	136.24	185.70	145.50	132.39	34.11	0	0
3	0	0	0	19.74	25.26	68.72	105.93	128.44	184.18	18.71	188.21	57.85	26.09	0	0	0
2	0	0	0	0	26.09	69.43	107.31	115.22	0	24.14	56.52	64.13	0	0	0	0
1	0	0	0	0	0	26.70	97.76	48.37	36.30	20.47	43.10	0	0	0	0	0
0	0	0	0	0	0	0	0	0	0	0	0	0	0	0	0	0

	0	1	2	3	4	5	6	7	8	9	10	11	12	13	14	15
15	0	0	0	0	0	0	0	0	0	0	0	0	0	0	0	0
14	0	0	0	0	0	0	0	0	0	0	1	0	0	0	0	0
13	0	0	0	0	0	0	0	0	50	0	0	0	0	0	0	0
12	0	0	0	0	0	0	1	0	0	0	0	0	0	0	0	0
11	0	0	1	3	0	1	2	1	1	77	1	3	4	78	0	0
10	0	0	119	16	53	23	167	43	57	114	234	141	82	30	131	0
9	0	0	75	96	140	63	165	80	40	76	20	99	48	12	120	0
8	0	0	82	74	135	18	0	16	18	50	14	61	62	8	28	0
7	0	0	8	44	10	1	14	20	20	26	37	61	73	4	4	0
6	0	5	15	51	10	55	32	63	7	31	44	61	46	59	37	0
5	0	4	48	31	45	70	36	48	28	12	46	44	31	57	37	0
4	0	0	33	39	32	64	15	38	43	62	51	42	6	98	0	0
3	0	0	0	56	35	62	46	51	8	65	40	7	23	0	0	0
2	0	0	0	0	54	34	81	58	0	34	16	75	0	0	0	0
1	0	0	0	0	0	3	46	55	34	6	67	0	0	0	0	0
0	0	0	0	0	0	0	0	0	0	0	0	0	0	0	0	0

APPENDIX I

MEASURED VERSUS PREDICTED COMPARISONS

This appendix contains 16 x 16 matrices of comparison values which are used to draw general observations and conclusions about the overall accuracy and consistency of the measured values obtained for this calibration. There is a separate spreadsheet for each star in each band.

The stated values were obtained using the simple percent error calculation of (predicted Lds - Measured Lds) divided by Predicted Lds. Negative values therefore indicate where the measured value exceeded the predicted value for a specific pixel. Values are only included for active pixels on the focal plane array and the letter 'M' indicates that no data was collected for that pixel. An 'E' is used in locations where the measured value differed from the predicted value by more than 90 percent.

2 Centauri in Band 1 (Compared)

	0	1	2	3	4	5	6	7	8	9	10	11	12	13	14	15
15							M	M	M	M						
14						0.5563	M	M	M	M	M					
13					0.1991	M	E	M	0.4843	M	E	E				
12				0.0906	E	E	M	M	M	E	M	M	M			
11			M	0.1665	0.0238	M	0.1373	M	M	M	M	0.7131	0.699	E		
10		M	0.0055	0.1625	0.0197	0.1163	0.0998	0.0545	0.1062	0.1345	0.0271	0.1764	0.2086	0.1794	0.4532	
9		E	0.2063	0.0688	0.0347	0.172	0.0383	0.0881	0.1485	0.124	0.1424	0.0957	0.1685	0.1489	0.5069	
8	M	0.2002	0.0877	0.0582	0.067	0.0216	0.1334	0.0811	0.1663	0.0768	0.0643	0.1828	0.1668	0.0406	0.2476	M
7	M	0.2178	0.1047	0.1041	0.0332	0.1546	0.1225	0.0795	0.0716	0.0665	0.2013	0.0704	0.1738	0.189	0.1078	M
6		0.4391	0.1104	0.0791	0.1053	0.102	0.1317	0.0595	0.0608	0.0265	0.0522	0.0367	0.1328	0.1582	0.6266	
5		E	0.154	0.0177	0.0786	0.0963	0.0239	0.0784	M	0.0054	0.0511	0.1092	0.0917	0.0769	0.5919	
4			0.3685	0.137	0.0503	0.0355	0.0669	0.1904	-0.005	0.14	-0.051	0.0932	0.094	0.5374		
3				0.3544	0.1708	0.1145	0.1295	0.1713	M	0.1368	0.0701	0.1457	0.4729			
2					0.5334	0.0726	0.1003	0.1727	0.0175	0.105	0.1515	0.5344				
1						0.5804	0.1503	0.1676	M	0.122	0.5347					
0							M	M	M	M						

2 Centauri in Band 2 (Compared)

	0	1	2	3	4	5	6	7	8	9	10	11	12	13	14	15
15							M	M	M	M						
14						0.6596	M	M	M	M	M					
13					0.691	M	M	M	0.2718	M	M	M				
12				0.4973	M	M	M	M	M	M	M	M	M			
11			0.4658	M	M	M	M	M	M	M	M	E	M	0.6869		
10		M	0.4544	0.4212	0.1347	0.3813	0.2237	M	0.2253	0.2851	0.4661	0.6605	0.3971	0.4215	0.6075	
9		0.4697	0.3577	0.3811	0.4417	0.3936	0.2101	0.3109	0.321	0.3697	0.2923	0.2823	0.3945	M	0.6914	
8	M	0.4908	M	0.32	M	0.4776	0.284	0.2233	0.2815	0.3988	0.3559	M	M	0.3714	M	M
7	M	0.5318	M	0.3251	M	0.3604	0.3223	0.3163	0.2443	0.3622	0.3736	0.4719	M	M	M	M
6		E	M	0.3504	M	0.334	0.2659	0.2037	0.1867	0.2878	0.4617	M	M	0.2352	0.6667	
5		0.6386	0.3794	0.4775	M	0.399	0.3598	0.2426	0.2648	0.2806	0.4281	0.3644	M	M	0.5595	
4			0.7695	M	0.3665	0.3338	0.2226	M	0.2865	M	0.3768	0.3552	M	0.6958		
3				0.782	0.3631	0.3749	0.1983	M	0.0887	M	0.4382	0.3322	0.6873			
2					0.6788	0.1995	0.201	M	0.3384	0.3037	0.5733	0.6344				
1						0.6804	0.3838	M	0.3768	M	0.6826					
0							M	M	M	M						

2 Centauri in Band 3 (Compared)

	0	1	2	3	4	5	6	7	8	9	10	11	12	13	14	15
15							M	M	M	M						
14						M	M	M	M	M	M					
13					M	M	E	M	0.0327	M	M	M				
12				M	0.2993	M	M	M	M	M	M	M	M			
11			M	0.1356	M	M	-0.093	-0.068	-0.154	0.0112	M	M	0.031	0.5962		
10		E	M	-0.009	-0.131	M	-0.193	-0.122	0.0708	-0.038	0.0985	0.1143	M	0.1892	0.6738	
9		M	0.151	0.0697	0.002	M	-0.041	-0.157	M	-0.121	0.1874	0.1257	0.0428	M	0.4967	
8	M	M	0.2186	0.0096	-0.082	-0.103	M	-0.161	0.0048	0.0665	0.106	0.0931	M	0.1141	M	M
7	M	M	0.129	0.0511	-0.127	-0.157	-0.245	M	-0.003	0.0874	0.0659	0.0879	-0.052	0.0951	M	M
6		M	0.181	M	-0.098	M	-0.201	-0.01	M	0.053	0.164	0.0893	M	0.094	0.3972	
5		M	0.1711	0.116	-0.036	M	-0.098	M	0.0112	0.0872	0.1244	0.0977	M	M	E	
4			0.4304	M	-0.029	-0.296	-0.152	M	M	0.0618	0.0787	0.0444	0.0753	0.6201		
3				0.6233	0.0165	M	-0.149	0.87	M	0.0142	M	M	0.5949			
2					0.2896	-0.076	-0.072	M	M	0.0618	0.1386	0.3344				
1						M	M	M	M	M	M					
0							M	M	M	M						

2 Centauri in Band 4 (Compared)

	0	1	2	3	4	5	6	7	8	9	10	11	12	13	14	15
15							M	M	M	M						
14					M	0.4341	M	0.4041	M	M	E					
13					0.6009	0.2933	-0.621	0.8011	M	-0.528	-0.33	-0.038				
12				0.6987	M	M	-0.583	-0.308	0.0032	-0.165	-0.661	-0.55	0.1897			
11			M	E	-0.286	0.4873	-0.309	-0.35	-0.527	-0.173	-0.102	-0.034	-0.291	0.1675		
10		M	M	-0.389	-0.635	-0.925	-0.432	-0.521	-0.293	-0.054	-0.106	0.1041	0.0532	-0.014	0.1907	
9		0.5392	M	M	-0.649	-0.405	-0.571	-0.429	-0.025	-0.425	-0.056	-0.156	0.1155	0.1522	0.4931	
8	M	0.7853	M	-0.308	-0.627	-0.738	-0.523	-0.378	-0.305	0.0754	-0.166	-0.151	-0.372	-0.082	-0.051	M
7	M	M	M	-0.695	-0.566	M	-0.792	-0.409	0.0586	-0.075	-0.39	-0.035	-0.297	0.0121	0.0918	M
6		0.5256	M	-0.248	-0.476	-0.871	-0.526	-0.112	-0.105	-0.172	-0.534	-0.135	-0.418	-0.187	-0.163	
5		0.553	M	-0.162	-0.494	-0.482	-0.292	-0.288	-0.185	-0.216	-0.198	-0.431	-0.555	-0.537	0.3474	
4			0.0125	0.1351	-0.299	-0.559	-0.374	-0.204	-0.118	-0.027	0.1045	-0.145	-0.461	0.2345		
3				0.1453	0.1328	-0.322	-0.227	0.0289	0.0002	0.191	-0.016	-0.339	0.2241			
2					0.2761	-0.03	-0.266	-0.332	0.08	-0.321	-0.219	0.2754				
1						0.3118	0.0315	0.0871	-0.049	0.395	0.2571					
0							M	M	M	M						

Alpha Centauri in Band 1 (Compared)

	0	1	2	3	4	5	6	7	8	9	10	11	12	13	14	15
15							M	M	M	M						
14						E	M	M	-0.378	M	M					
13					M	M	M	-0.236	0.3911	M	E	E				
12				M	M	0.1029	-0.213	-0.154	0.8523	M	M	0.5151	M			
11			M	-0.068	-0.13	-0.097	-0.064	-0.131	-0.261	-0.181	-0.216	-0.163	-0.114	0.1759		
10		E	M	-0.136	-0.149	-0.095	-0.169	-0.158	-0.316	E	-0.254	-0.132	-0.126	-0.082	0.2244	
9		E	E	-0.298	-0.199	-0.093	-0.181	-0.107	-0.164	-0.251	-0.2	-0.16	-0.16	-0.1	0.0459	
8	M	E	E	-0.377	-0.197	-0.132	0.1146	0.0962	0.2092	-0.162	-0.336	-0.121	-0.146	M	-0.022	M
7	M	M	M	-1.028	-0.121	-0.103	0.152	0.2045	E	-0.146	-0.192	-0.181	-0.132	-0.155	-0.1	M
6		M	M	-0.273	-0.061	0.0285	0.2251	M	0.1779	-0.15	-0.094	-0.156	-0.224	-0.09	0.702	
5		M	M	-0.213	-0.056	-0.056	-0.121	E	E	-0.179	-0.163	-0.166	-0.168	-0.045	0.2497	
4			E	-0.234	-0.086	E	E	-0.133	-0.256	E	M	-0.264	-0.088	0.3742		
3				0.4027	-0.081	0.0713	-0.101	-0.202	-0.197	-0.155	-0.373	E	0.5503			
2					0.3275	M	-0.03	-0.089	-0.303	E	-0.21	0.2648				
1						0.4359	M	-0.188	-0.142	-0.046	0.3472					
0							M	M	M	M						

Alpha Centauri in Band 2 (Compared)

	0	1	2	3	4	5	6	7	8	9	10	11	12	13	14	15
15							M	M	M	M						
14						M	M	M	M	M	M					
13					E	M	0.7051	M	0.4146	M	M	E				
12				E	M	0.3005	M	0.2258	M	0.9752	M	0.871	M			
11			M	0.011	-0.145	-0.237	-0.286	-0.292	-0.341	-0.28	-0.164	-0.192	-0.245	0.0266		
10		E	0.1914	M	-0.227	-0.28	-0.252	-0.307	-0.315	-0.299	-0.287	-0.249	-0.238	-0.186	0.5301	
9		E	M	-0.305	-0.23	-0.245	-0.19	-0.246	-0.243	-0.33	-0.207	-0.214	-0.247	-0.24	0.282	
8	M	M	-0.037	-0.156	-0.234	-0.276	-0.214	-0.219	-0.205	-0.363	-0.17	-0.305	M	-0.249	-0.221	M
7	M	M	M	-0.098	-0.331	-0.183	-0.271	-0.24	-0.273	-0.381	-0.263	M	M	-0.217	0.7821	M
6		E	M	-0.114	-0.231	-0.206	-0.346	-0.413	-0.162	-0.245	-0.263	-0.174	-0.141	-0.383	0.5667	
5		M	M	-0.091	-0.092	-0.191	-0.23	-0.242	-0.246	-0.385	-0.171	-0.801	-0.239	-0.211	0.6086	
4			E	-0.141	-0.107	-0.175	-0.246	-0.218	-0.269	-0.213	-0.243	-0.228	-0.202	0.2854		
3				0.4138	-0.152	-0.204	-0.233	-0.273	-0.168	-0.201	-0.247	-0.23	-0.003			
2					0.2798	-0.236	-0.129	-0.265	-0.079	-0.205	-0.209	-0.003				
1						0.065	-0.108	-0.217	-0.173	-0.142	0.367					
0							M	M	M	M						

Alpha Centauri in Band 3 (Compared)

	0	1	2	3	4	5	6	7	8	9	10	11	12	13	14	15
15							M	M	M	M						
14						M	-0.347	-0.596	M	M	M					
13					-0.489	-0.641	M	M	0.2632	M	M	M				
12				-0.528	E	M	M	M	M	M	M	M	M			
11			-0.544	-0.628	-0.603	-0.62	-0.605	-0.585	-0.647	-0.561	-0.56	-0.594	-0.601	0.3464		
10		M	-0.596	-0.605	-0.597	-0.483	-0.521	-0.603	-0.56	-0.572	-0.521	M	-0.492	-0.532	0.4403	
9		M	-0.536	-0.606	-0.623	-0.505	-0.526	-0.565	-0.583	-0.626	-0.569	-0.491	-0.553	M	0.3343	
8	M	M	-0.582	-0.551	-0.578	-0.555	-0.557	-0.533	-0.63	-0.561	-0.526	-0.523	-0.508	E	-0.086	M
7	M	M	-0.58	-0.553	-0.609	-0.635	-0.571	-0.487	-0.673	-0.626	-0.566	-0.459	-0.598	M	-0.512	M
6		E	-0.566	-0.629	-0.617	-0.624	-0.569	-0.602	-0.658	-0.458	-0.469	-0.533	-0.533	-0.54	-0.339	
5		M	-0.618	-0.522	-0.646	-0.567	-0.559	-0.595	-0.644	-0.574	-0.557	-0.514	-0.577	-0.615	-0.248	
4			-0.196	-0.551	-0.677	-0.613	-0.639	-0.576	-0.612	-0.655	-0.614	-0.602	-0.393	0.0681		
3				-0.269	-0.638	-0.559	-0.704	-0.592	-0.592	-0.611	-0.371	-0.513	0.3573			
2					-0.122	-0.573	-0.547	-0.583	-0.607	-0.543	-0.417	-0.288				
1						-0.067	-0.539	-0.563	-0.525	-0.458	-0.141					
0							M	M	M	M						

Gamma Crucis in Band 1 (Compared)

	0	1	2	3	4	5	6	7	8	9	10	11	12	13	14	15
15							M	M	M	M						
14						M	M	M	M	M	M					
13					E	M	M	M	E	M	M	M				
12				M	M	M	M	M	M	M	M	E	M			
11			M	0.036	M	0.005	0.066	0.005	0.034	0.084	0.012	0.057	0.011	0.093		
10		0.747	0.036	0.034	0.073	0.022	0.028	-0.006	0.052	0.076	0.02	0.025	0.014	0.008	0.648	
9		0.409	0.002	0.02	0.078	-0.001	-0.006	0.015	-0.018	0.005	0.064	M	-0.017	0.016	0.064	
8	M	0.352	0.021	0.057	0.044	0.235	0.321	-0.009	-0.024	-3E-04	0.072	0.567	0.01	0.031	M	M
7	M	0.393	0.003	0.056	0.048	0.277	0.326	0.009	-0.01	0.004	0.075	0.825	0.052	0.046	M	M
6		0.515	0.068	0.032	-0.013	0.246	0.459	0.059	0.087	0.039	0.02	0.568	0.021	0.033	M	
5		0.486	0.091	0.018	-0.009	0.069	-0.005	0.054	0.087	0.068	0.049	0.058	0.017	0.069	0.452	
4			0.473	0.065	0.021	0.023	-0.03	-0.001	0.014	0.07	-0.004	0.054	0.007			
3				0.364	0.049	0.086	0.027	0.024	0.017	0.056	0.023	0.011	0.494			
2					0.536	0.116	0.028	0.056	0.012	0.009	0.075	0.341				
1						0.767	0.049	0.079	0.022	0.063	0.441					
0							M	M	M	M						

Gamma Crucis in Band 2 (Compared)

	0	1	2	3	4	5	6	7	8	9	10	11	12	13	14	15
15							M	M	M	M						
14						M	E	M	M	M	M					
13					E	M	M	M	0.7674	M	M	M				
12				M	M	M	0.8208	0.8711	M	M	0.8137	M	M			
11			0.6771	M	M	M	M	0.1871	0.1857	0.1814	0.2	0.2377	0.1836	0.4055		
10		0.2831	M	M	M	E	M	0.1856	0.1838	0.1699	0.1957	0.1804	0.1958	0.1979	M	
9		0.3494	0.4711	M	M	M	M	0.1817	0.1763	0.1703	0.2728	0.1713	0.239	0.2238	M	
8	M	0.2369	0.2086	M	M	M	M	0.16	0.1732	0.1865	0.2184	0.1851	0.2366	0.2042	M	M
7	M	0.2303	M	M	M	M	M	0.1782	0.1615	0.1759	0.1603	0.1839	0.2394	0.2738	M	M
6		0.2366	M	M	M	M	0.1945	0.1827	0.206	0.1966	0.2006	0.202	0.2227	0.2577	M	
5		0.2367	M	M	M	M	0.1939	0.1876	0.2003	0.1916	0.1859	0.1963	0.2253	0.2099	M	
4			0.819	M	0.8118	M	0.1847	0.1911	0.2131	0.2012	0.213	0.1793	0.2409	0.3688		
3				M	M	M	M	0.1871	0.2111	0.2222	0.203	0.2048	0.3728			
2					M	E	M	0.1834	0.1877	0.2272	0.2119	0.4155				
1						M	E	0.2187	0.2169	0.2231	0.5188					
0							M	M	M	M						

Gamma Crucis in Band 3 (Compared)

	0	1	2	3	4	5	6	7	8	9	10	11	12	13	14	15
15							M	M	M	M						
14						M	M	M	M	M	M					
13					M	M	M	M	E	M	M	M				
12				M	M	M	M	E	M	M	E	M	M			
11			0.1772	-0.073	-0.082	-0.049	-0.081	-0.11	-0.111	-0.079	-0.075	-0.036	M	0.6847		
10		0.34	-0.072	-0.111	-0.106	-0.096	-0.072	-0.113	-0.122	-0.144	-0.118	-0.125	-0.095	-0.109	0.2884	
9		0.6057	-0.058	-0.111	-0.111	-0.162	-0.084	-0.117	-0.124	-0.139	-0.095	-0.106	-0.132	-0.058	M	
8	M	0.0349	-0.121	-0.057	-0.137	-0.102	-0.074	-0.108	-0.083	-0.129	-0.089	-0.109	-0.101	-0.155	M	M
7	M	0.1034	-0.135	-0.106	-0.145	-0.07	-0.092	-0.152	-0.121	-0.072	-0.097	-0.117	-0.158	-0.112	M	M
6		0.546	-0.084	-0.117	-0.163	-0.079	-0.13	-0.125	-0.106	-0.104	-0.123	-0.175	-0.137	M	-0.016	
5		0.6671	-0.081	-0.052	-0.112	-0.153	-0.132	-0.095	-0.105	-0.118	-0.135	-0.105	-0.148	-0.087	-0.077	
4			0.3491	-0.135	-0.106	-0.151	-0.14	-0.087	-0.119	-0.129	-0.107	-0.147	-0.134	0.3709		
3				E	-0.097	-0.074	-0.112	-0.153	-0.072	-0.124	-0.002	-0.126	0.2924			
2					-0.032	-0.106	-0.091	-0.092	-0.111	-0.113	-0.122	0.4273				
1						0.3702	-0.085	-0.073	-0.08	-0.055	0.1535					
0							M	M	M	M						

Lambda Velorum in Band 1 (Compared)

	0	1	2	3	4	5	6	7	8	9	10	11	12	13	14	15
15							M	M	M	M						
14						M	M	M	M	M	M					
13					M	M	M	M	0.7762	M	M	M				
12				M	M	M	M	E	M	0.827	M	M	M			
11			M	0.6644	M	0.7974	0.778	0.6871	0.6721	0.7474	0.7777	0.774	0.7257	0.8677		
10		M	0.6529	0.742	0.812	0.7782	0.7372	0.69	0.7011	0.7371	0.7511	0.7195	0.7306	0.7382	0.8487	
9		M	0.657	0.7374	0.7965	0.7587	0.858	0.712	0.7121	0.7592	0.739	0.7184	0.731	0.7425	0.8303	
8	M	E	0.6486	0.7785	0.794	0.7795	0.7093	0.7132	0.7181	0.7399	0.7423	0.7164	0.7396	0.743	0.7623	M
7	M	M	0.6774	0.773	0.7864	0.7707	0.683	0.7126	0.6818	0.7587	0.753	0.7197	0.7295	0.7477	0.7435	M
6		E	0.6765	0.7553	0.7927	0.7612	0.6867	0.717	0.7188	0.755	0.747	0.7031	0.7088	0.7486	0.8085	
5		E	0.7034	0.7864	0.7858	0.7529	0.6708	0.7227	0.7233	0.751	0.7379	0.7232	0.7179	0.7441	0.8572	
4			0.7074	0.7717	0.7833	0.7417	0.6547	0.7396	0.7083	0.7441	0.7355	0.7031	0.7326	0.7767		
3				0.8413	0.7807	0.748	0.6505	0.7298	0.7294	0.7573	0.7479	0.7166	0.8421			
2					0.7978	0.7491	0.6667	0.7184	0.6678	0.7635	0.7386	0.7611				
1						0.8084	0.6622	0.6292	0.7508	0.7634	0.7939					
0							M	M	M	M						

Lambda Velorum in Band 2 (Compared)

	0	1	2	3	4	5	6	7	8	9	10	11	12	13	14	15
15							M	M	M	M						
14						0.858	0.7564	0.7189	M	0.6658	M					
13					M	M	M	M	0.6984	M	M	M				
12				M	M	M	0.6699	M	M	0.7512	M	M	0.82			
11			0.7847	E	0.8958	0.6816	0.6613	0.7029	0.8184	0.8172	0.6846	0.6397	0.7477	E		
10		0.847	0.8108	E	0.8221	0.6834	0.7523	0.7241	0.835	0.5909	0.7113	0.7492	0.8272	0.8412	0.8372	
9		E	E	0.8571	0.7577	0.6812	0.749	0.7823	0.6477	0.7408	0.6131	0.7671	0.8271	0.6047	0.8215	
8	M	M	E	0.8297	0.7184	0.6877	0.8114	0.8218	0.7936	0.684	0.754	0.7017	0.8153	0.6915	0.7387	M
7	M	M	E	0.8223	0.7015	0.6941	0.8027	0.8044	0.73	0.6267	M	0.7477	0.825	0.6649	0.8219	M
6		M	E	0.8235	0.7597	0.7026	0.7856	0.6763	0.7897	0.6135	0.7512	0.6381	0.8208	0.8094	0.8191	
5		M	E	0.829	0.811	0.7155	0.6879	0.7115	0.6427	0.7164	0.6268	0.7432	0.8183	0.8227	0.8409	
4			E	E	0.8325	0.6745	0.8319	0.7506	0.7983	0.6716	0.7463	0.6754	0.812	0.8522		
3				E	E	0.6557	0.7541	0.8446	0.843	0.7808	0.6315	0.786	0.854			
2					E	0.7458	0.5054	0.8185	0.8391	0.7063	0.7472	E				
1						0.7434	0.788	0.8408	0.8215	0.7699	0.6996					
0							M	M	M	M						

Lambda Velorum in Band 3 (Compared)

	0	1	2	3	4	5	6	7	8	9	10	11	12	13	14	15
15							M	M	M	M						
14						M	E	M	M	M	M					
13					M	M	0.6637	E	0.595	M	M	M				
12				M	M	0.6829	0.774	0.4755	M	0.7515	M	E	M			
11			M	0.696	E	0.7657	0.7259	0.5167	M	M	E	0.5089	0.619	0.7662		
10		M	0.6957	0.7399	0.8242	0.7255	0.5135	0.5198	M	M	M	0.5468	0.6268	0.6716	E	
9		0.6532	0.7551	0.8016	0.8276	0.709	0.5382	0.5247	0.7898	E	0.5908	0.9414	0.4719	0.735	0.7939	
8	M	0.6747	0.725	0.7565	0.8298	0.7244	0.6729	0.5196	0.907	M	0.602	M	0.4621	0.6851	0.6908	M
7	M	0.5671	0.7795	0.7955	0.8054	E	E	0.5778	M	M	0.6338	0.6215	0.6425	0.6708	0.6999	M
6		0.6005	0.7566	0.8067	0.8437	0.6861	0.6991	0.5824	M	M	0.6634	0.6248	0.6055	0.6978	0.7539	
5		0.7175	M	0.8104	E	0.9279	0.7442	0.616	0.6311	M	M	0.6353	0.6024	0.6903	0.8317	
4			0.7408	0.7682	0.7515	0.7243	0.7237	0.6211	M	M	M	0.6471	0.6611	0.7808		
3				0.8496	0.7172	0.7719	0.722	0.5971	M	E	0.6097	0.7335	0.7105			
2					0.8236	0.7854	0.7305	M	M	M	0.4823	0.7912				
1						0.8059	0.6013	M	M	E	0.7957					
0							M	M	M	M						

Lambda Velorum in Band 4 (Compared)

	0	1	2	3	4	5	6	7	8	9	10	11	12	13	14	15
15							M	M	M	M						
14						M	M	M	M	M	0.786					
13					M	M	M	M	-0.123	M	M	M				
12				M	M	M	0.1181	M	M	M	M	M	M			
11			0.2906	0.1782	M	0.3254	0.0071	0.3206	0.8056	0.7683	0.7375	E	0.6534	0.7731		
10		M	0.5275	0.7214	M	0.342	0.3674	0.4993	0.0385	E	0.8211	0.5541	0.4924	0.6359	0.7974	
9		M	0.6224	M	M	0.7707	0.1353	0.0846	0.6816	E	0.0796	-0.124	0.6243	0.4346	0.7646	
8	M	M	0.4163	M	E	E	M	0.5793	0.1519	-0.164	0.0205	0.5716	0.5526	0.495	0.7441	M
7	M	M	E	M	M	E	0.1992	0.5593	-0.067	-0.017	-0.254	0.527	0.6194	0.4078	0.5363	M
6		0.4011	0.8432	M	E	E	0.1453	0.5049	0.5754	-0.129	0.7526	-0.27	0.637	-0.099	E	
5		0.6928	0.7957	E	E	0.5806	0.1681	0.1724	-0.389	-0.187	0.6643	-0.045	0.5887	0.7032	0.7983	
4			0.8201	E	E	0.6154	0.2954	0.2682	0.8339	0.1485	-0.161	0.0906	0.1726	0.7868		
3				E	0.8421	0.5705	0.3379	0.1973	-0.151	E	-0.176	0.6384	0.8369			
2					0.8369	0.5661	0.3293	0.2799	M	0.8491	0.6468	0.5992				
1						0.8331	0.389	0.6977	0.7731	E	0.7306					
0							M	M	M	M						

BIBLIOGRAPHY

1. C. W. Engelke, "Analytic approximations to the 2-60μm infrared continua for standard calibration stars: with application to the calibration of spectroscopy and photometry, and the determination of effective temperature and angular size from IR measurements", Astronomical Journal **104**(3), 1248-1258, Sep 92

2. C. W. Engelke, *LWIR Stellar Calibration: Infrared Spectral Curves for 30 Standard Stars*, MIT Lincoln Lab, AD-A236766, Apr 91

3. W. Stupak, Private communication, Jul 95

4. J. M. Sorvari, *A Proposed Astronomical Reference Catalog Of Infrared Sources*, Massachusetts Institute of Technology Lincoln Laboratory, ESD-TR-90-085, 6 Aug 90

5. J. A. Thomas, A. R. Hyland, and G. Robinson, "Southern infrared standards and the absolute calibration of infrared photometry", Monthly Notices of the Royal Astronomical Society, (165), 201-211, (1973)

6. M. Cohen, R. Walker, et al., "Spectral irradiance calibration in the infrared. I. ground-based and IRAS broadband calibrations", The Astronomical Journal **104**(4), 1650-1657, Oct 92

7. M. Cohen, private communication, Jan 96

8. R. L. Cody, Private communication, Jun 95

9. C. N. Vittitoe, J. D. George, *Focal-plane array corrections for optical data*, Sandia National Labs, 28 Aug 95

10. G. J. Zissis, et al., *The Infrared and Electro-Optical Systems Handbook: Volume 1 - Sources of Radiation*, ERIM and SPIE, (1993)

11. W. D. Dong, Unpublished Paper, Hughes Aircraft Company, 1994

12 C. W. Allen, *Astrophysical Quantities*, The Athlone Press, 3rd ed. (1976)

13. *Smithsonian Physical Tables*, Smithsonian Institution, 9th ed. (1954)

14. R. Kingslake, *Applied Optics and Optical Engineering*, Volume 1, "Light and Its Generation and Modification", Academic Press (1965)

15. J. Engel, Private communication, Jan 96

16. C. L. Wyatt, *Radiometric Calibration: Theory and Methods*, Academic Press, (1978)

17. B. Borowski, unpublished fact sheet for processing software, Feb 96

18. R.L. Cody, private communication, Sep 96

19. Rockwell International Corporation, "Sensor Description", (unpublished document)

20. R. C. Ramsey, "Spectral Irradiance from stars and planets, above the atmosphere, from 0.1 to 100.0 microns", Applied Optics **(1)**4, Jul 62

21. D. Y. Gezari, et. al, *Catalog of Infrared Observations (Third Ed.)*, National Aeronautics and Space Administration, Jun 93

22. B. Parker, private communication, Sep 95 - Jan 96

23. M. Cohen, et. al, "Spectral irradiance calibration in the infrared. VI. 3-35mm spectra of three standard stars", The Astronomical Journal, **112**(1), 241-251, Jul 96

24.. B. Borowski, unpublished source code listings for processing programs, Feb 96

25. J. J. Lisowski, private communication, Jun 95